(This is a sample cover image for this issue. The actual cover is not yet available at this time.)

Journal of Nuclear Materials 420 (2012) 409–423

Contents lists available at SciVerse ScienceDirect

Journal of Nuclear Materials

journal homepage: www.elsevier.com/locate/jnucmat

Review

Radiation induced dissolution of UO_2 based nuclear fuel – A critical review of predictive modelling approaches

Trygve E. Eriksen [a], David W. Shoesmith [b], Mats Jonsson [a,*]

[a] KTH Chemical Science and Engineering, Nuclear Chemistry, Royal Institute of Technology, SE-100 44 Stockholm, Sweden
[b] Department of Chemistry, University of Western Ontario, London, Ontario, Canada N6A 5B7

ARTICLE INFO

Article history:
Received 25 November 2010
Accepted 18 October 2011
Available online 6 November 2011

ABSTRACT

Radiation induced dissolution of uranium dioxide (UO_2) nuclear fuel and the consequent release of radionuclides to intruding groundwater are key-processes in the safety analysis of future deep geological repositories for spent nuclear fuel. For several decades, these processes have been studied experimentally using both spent fuel and various types of simulated spent fuels. The latter have been employed since it is difficult to draw mechanistic conclusions from real spent nuclear fuel experiments. Several predictive modelling approaches have been developed over the last two decades. These models are largely based on experimental observations. In this work we have performed a critical review of the modelling approaches developed based on the large body of chemical and electrochemical experimental data. The main conclusions are: (1) the use of measured interfacial rate constants give results in generally good agreement with experimental results compared to simulations where homogeneous rate constants are used; (2) the use of spatial dose rate distributions is particularly important when simulating the behaviour over short time periods; and (3) the steady-state approach (the rate of oxidant consumption is equal to the rate of oxidant production) provides a simple but fairly accurate alternative, but errors in the reaction mechanism and in the kinetic parameters used may not be revealed by simple benchmarking. It is essential to use experimentally determined rate constants and verified reaction mechanisms, irrespective of whether the approach is chemical or electrochemical.

Contents

* Corresponding author. Tel.: +46 8 790 9123; fax: +46 8 790 8772.
E-mail address: matsj@kth.se (M. Jonsson).

0022-3115/$ - see front matter © 2011 Elsevier B.V. All rights reserved.
doi:10.1016/j.jnucmat.2011.10.027

1. Introduction

The safety analysis of future deep geological repositories for spent nuclear fuel relies on extensive extrapolations of models describing the numerous processes affecting the release into, and mobility of radionuclides in, the geosphere/biosphere. One of the key processes is the release of radionuclides from spent nuclear fuel in contact with groundwater inside a failed waste container. In general, the UO_2 matrix containing the radioactive fission products and actinides has a very low solubility in groundwater [1]. However, the inherent radioactivity of spent nuclear fuel causes the emission of α-, β- and γ-radiation which will be absorbed by the water adjacent to the fuel surface giving rise to its radiolytic decomposition [2]. Radiolysis of water produces both oxidants and reductants capable of altering the fuel matrix. As the spent nuclear fuel matrix is in its reduced (U(IV)) form, radiolytic oxidants will, at least during the early stages, have higher impact than their reducing counterparts. Oxidation of the fuel matrix will produce U(VI) which is considerably more soluble than the reduced form [3] and will lead to its enhanced dissolution, and, thereby, to the release of radionuclides.

The overall process of oxidative dissolution (corrosion) of solid UO_2 involves a sequence of oxidation, dissolution, and possibly, under certain conditions, deposition reactions. At a macroscopic level the process can be described by the sequence

$$UO_2 \rightarrow UO_{2+x} \rightarrow UO_2^{2+} \rightarrow UO_3 \cdot yH_2O \quad (1)$$

where UO_{2+x} ($U^{IV}_{1-2x}U^{V}_{2x}O_{2+x}$) is a thin intermediate oxidized layer on the UO_2 surface [3], and $UO_3{\cdot}yH_2O$ is a U^{VI} deposit formed if local supersaturation with dissolved UO_2^{2+} occurs at the fuel surface. Since most repository groundwaters have a pH in the range 7–10, when U^{VI} solubility is at a minimum, redeposition of dissolved UO_2^{2+} is likely to occur, unless the groundwater has a significant HCO_3^-/CO_3^{2-} content, when U^{VI} complexation

$$UO_2^{2+} + aHCO_3^- \rightarrow UO_2(HCO_3)_a^{2-a} \quad (2)$$

will increase the solubility and prevent redeposition of UO_2^{2+}, thereby accelerating the oxidative dissolution kinetics [4]. If deposition is avoided, then the steady-state oxidative dissolution process can be adequately described as a two step reaction occurring on the UO_{2+x} surface layer,

$$Ox + UO_2 \rightarrow Red + UO_2^{2+}(surf) \quad (3)$$

$$UO_2^{2+}(surf) \rightarrow UO_2^{2+}(aq) \quad (4)$$

In the presence of UO_2^{2+} complexing agents such as HCO_3^-, the release of UO_2^{2+} from the surface to the solution (dissolution reaction (4)) is enhanced and the overall reaction becomes limited by the rate of oxidation (reaction (3)).

Both electrochemical [3,5,6] and chemical studies [7–9] yield consistent results showing that, for a carbonate concentration $\geqslant 10^{-3}$ mol dm^{-3} the formation of significant amounts of U^{VI} deposits is prevented and oxidative dissolution proceeds uninhibited at a much higher rate than in the absence of carbonate. As the carbonate concentration is increased, both deposition and formation of the underlying UO_{2+x} layer are prevented [7,9] and oxidative dissolution facilitated [6].

While carbonate is expected to be the dominant groundwater species influencing oxidative fuel dissolution, other species, such as Ca^{2+} and silicate, which exert a considerable influence on uranium mineralogy [10], are likely to promote the formation of deposits. The formation of secondary phases involving these ions, and other cations (K^+, Na^+) has been extensively characterized under the oxidizing conditions anticipated in the proposed Yucca Mountain repository (Nevada, USA) [11] but has received minimal attention under the less oxidizing conditions anticipated in granitic and sedimentary clay repositories [12,13].

Considerable effort has been expended to develop models to predict oxidative dissolution. These models must account for the geometrical dose distribution (i.e., the radiation dose as a function of distance from the fuel surface), surface reactions such as oxidation and dissolution, diffusion due to the inherent concentration gradients imposed by the geometrical dose distribution as well as the surface reactions and the chemistry of the bulk UO_2 phase. The formation of secondary solid phases constitutes an additional problem that is particularly difficult to address. Issues arising due to the accumulation of these deposits would include: (i) an unpredictable reduction in the surface area of fuel available for dissolution; (ii) the restriction of diffusion processes, in particular of radiolytic oxidants from, and potential oxidant scavengers (Fe^{2+}, H_2) to, the fuel surface; (iii) the co-precipitation of alpha emitters released by fuel dissolution [14,15].

The reliability of a model depends on the extent to which it accounts for relevant processes and parameters, and to what extent it is based on unverified assumptions, not supported by experimental data. Data from experiments on spent nuclear fuel as well as simpler simulated fuels constitute the basis for model development as well as providing a means to validate (benchmark) the models. Hence, access to reliable experimental data is of vital importance. In this paper, we critically review existing modelling approaches in view of the available experimental data and current mechanistic understanding. Due to the lack of kinetic data on dissolution and precipitation processes in systems limited by solubility, we focus on systems where dissolution can be represented by reactions (3) and (4).

Before discussing the body of experimental work and scrutinizing the proposed modelling approaches it is essential to summarize the fundamentals of some of the unique features of the system of interest and some of the experimental techniques used.

1.1. Radiolysis of aqueous solutions

The mechanism for energy absorption by aqueous solutions depends on the type of radiation [2]. Heavy, highly charged particles (i.e. He^{2+}) interact strongly with the absorbing medium. Hence, their penetration depth is short and the energy is deposited in a small volume of the absorber. Due to the high particle mass the deflection caused by interacting coulomb fields is small, leading to straight paths. Furthermore, the secondary electrons produced have relatively low energy and only a minor fraction cause secondary ionization [16,17]. Lighter, less charged particles (i.e., electrons) have longer penetration depths and are more widely scattered out of the incident beam path. Electromagnetic radiation (i.e. γ-photons) interacts very sparsely with water due to the absence of charge and mass. Consequently, the penetration depth is much longer and all the energy is lost in one, or a few, interactions.

The ionization caused by γ-absorption is almost completely due to secondary ionization. The radiation chemical yield is described in terms of *G*-values, which are the number of moles of the irradiated material transformed per Joule of absorbed energy (mol J^{-1}) [16,17]. The yields depend on the type of radiation and the energy.

In a heterogeneous system, energy, charge and matter can be transported through the interface. This, as well as catalytic and steric effects, could alter the process of water decomposition. In radiation-induced oxidative dissolution of spent nuclear fuel, the central reaction is between radiolysis products and the fuel surface. Hence, it is of crucial importance to elucidate the effects of the presence of a solid surface on the yield of water radiolysis products. LaVerne et al. [18–21] have studied radiolytic H_2 production in the presence of solid oxide surfaces. Some of these studies were on thin films of water on oxide surfaces, and others on powder suspensions or slurries. In general, *G*-values were found to increase with decreasing number of water layers on the surface, probably by transfer of energy originally deposited in the solid phase to the liquid phase. The effect clearly depends on the type of oxide and its surface morphology. Experiments on slurries and suspensions show that very high solid-surface-area-to-solution-volume (*A*/*V*) ratios are required to significantly increase the *G*-value for H_2 above that for bulk water [19]. For SiO_2 in water an *A*/*V* ratio of $\sim 10^7$ m^{-1} is required to observe an effect on the *G*-value [19]. This corresponds to a water layer with a thickness of ca 60 nm, i.e., a thickness significantly shorter than the maximum range of α-particles in water (30–40 μm). The *A*/*V* ratio in the oxidative dissolution of spent nuclear fuel in aqueous solution is several orders of magnitude lower than this, making the surface-enhanced H_2 production unimportant [22].

Radiolytic production of H_2O_2 does not appear to be affected by the presence of oxide surfaces to the same extent as H_2 [18]. A key unresolved issue is the influence of radiation, especially alpha, when the surface is covered with a porous deposit whose thickness is greater than the penetration depth of the particle in water and which possesses water-filled pores. Under these conditions, the *A*/*V* ratio in confined pores could exceed 10^7 m^{-1} and the apparent radiation chemical yields could deviate from the bulk values.

1.2. Kinetics of heterogeneous systems

As for homogeneous bimolecular reactions, collision theory can also be used to describe the kinetics of interfacial reactions between a solid surface and solutes in the liquid phase. Astumian and Schelly have described the theory for the kinetics of interfacial reactions in detail [23]. The complete rate expression for solutes reacting with suspended solid spherical particles is given by:

$$\frac{d[Solute]}{dt} = -\frac{2k_BT}{3\pi\eta}\frac{R_{SolidMol}^2}{R_{Solute}R_P}\left(e^{-\frac{E_a}{RT}}\right)[Solute]\frac{N_{SolidMol}}{V} \quad (5)$$

where k_B denotes the Boltzmann constant, η is the viscosity of the solvent, $R_{SolidMol}$ is the radius of the molecules constituting the solid material, R_{Solute} is the molecular radius of the reacting solute, R_P is the radius of the solid particle, $N_{SolidMol}$ is the number of molecules on the surface of the solid being exposed to the solution of volume *V*. In accordance with conventional collision theory for homogeneous bimolecular reactions, the part of the expression preceding the reactant concentrations can be identified as the rate constant. From this expression it can be seen that with increasing particle size the diffusion controlled rate constant (collision frequency) decreases. As a consequence, the maximum rate constant decreases with increasing size of the solid particle.

In practice, the *A*/*V* ratio is often used to quantify the amount of solid reactant. Therefore, experimentally determined second order rate constants for interfacial reactions have the unit m s^{-1}. As the true surface area of the solid is very difficult to determine, the value obtained in BET measurements is frequently used. The maximum diffusion controlled rate constant for a particle suspension containing μm-sized particles is ca 10^{-3} m s^{-1}, and for mm-sized particle suspensions the corresponding value is 10^{-6} m s^{-1} [22]. Consequently, it is very important to apply the correct rate constants when simulating the kinetics of a heterogeneous system. Diffusion limited rate constants for heterogeneous systems can also be derived from electrode kinetics resulting in comparable values [24].

Rate constants for interfacial reactions have mainly been determined from experiments using particle suspensions where the concentration of reactive solute is monitored as a function of time [25]. In these experiments, the *A*/*V* ratio is very large and the consumption of reactive solute follows first order kinetics. By plotting the pseudo first order rate constant against the *A*/*V* ratio the second order rate constant can be obtained (from the slope). The main limitation is that only relatively stable solutes can be studied experimentally. It is not possible to study the reactivity of short-lived species such as radicals using this approach.

The rate of reactive solute consumption is given by:

$$-\frac{d[Solute]}{dt} = k_1\left(\frac{A}{V}\right)[Solute] \quad (6)$$

While the rate of surface reaction is given by:

$$-\frac{dn_{surface}}{dt} = k_1(A)[Solute] \quad (7)$$

Here *A* denotes the solid surface area, and *V* is the solution volume.

1.3. Electrochemistry of oxidative dissolution [24]

As mentioned above, the oxidative dissolution of UO_2 in the presence of radiolytic oxidants is a corrosion reaction, the thermodynamic driving force for which can be expressed in terms of the difference in equilibrium potentials (E^e, defined by the Nernst equation) for fuel oxidation/dissolution and the redox potential of the solution close to the surface. Under these conditions, the fuel will establish a corrosion potential (E_{CORR}) at which the anodic dissolution rate ($UO_2 \rightarrow UO_2^{2+} + 2e^-$), termed the corrosion rate, is equal to the rate of the oxidant reduction reaction (Ox + 2-e^- → Red). Since both of these half reactions occur on the UO_2 surface, no net current flows in any external measuring circuit, meaning the corrosion (oxidative dissolution) rate cannot be straightforwardly measured using conventional electrochemical methods. However, the use of probe electrodes enables direct measurement of corrosion rates.

While each of these half reactions (the overall reaction is the sum of the two) would be reversible at its respective equilibrium potential, under corrosion conditions (i.e., at E_{CORR}) they are polarized away from their respective E^e values, to a degree given by $E^e \pm E_{CORR}$, and are generally irreversible. The extent to which each half reaction is polarized is determined by the relative kinetics of the half reactions, and the most polarized reaction (i.e., the one demanding the largest fraction of the difference between equilibrium potentials) is the kinetically slowest. Because it is determined by distinct half reactions, E_{CORR} is commonly referred to as a mixed potential. This coupling of half reactions is illustrated for radiolytically-produced H_2O_2 in Fig. 1. It is obvious that this simple coupling of half reactions will become much more complicated if more than one radiolytic oxidant (or reductant) is involved and/or the corroding surface is partially covered by re-deposited corrosion products (e.g., $UO_3{\cdot}yH_2O$).

The rate of an electrochemical reaction can be expressed by a rate law identical to that used for a chemical reaction providing

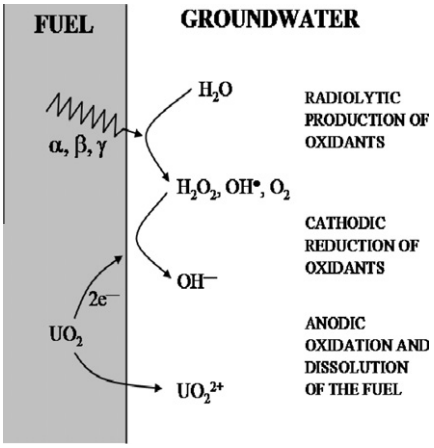

Fig. 1. Illustration showing the radiolytic production of oxidants by the radiolysis of water, and the coupling of cathodic oxidant processes to anodic fuel dissolution which constitutes the overall fuel corrosion process.

two additional features are acknowledged: (i) the reaction involves the destruction of a surface and its rate will, therefore, be limited by the available reactive surface area; (ii) the rate constant is exponentially-dependent on the electrochemical potential. Thus, for a reagent R in solution, we can write the rate expression

$$-d[R]/dt = k[R]^p = i/nFA \tag{8}$$

in which i is the current, n is the number of electrons involved (2 for UO_2 dissolution as UO_2^{2+}) and F is the Faraday constant. Using this relationship, and including the exponential dependence of the rate constant on electrochemical potential, the rate for the anodic dissolution of UO_2 (i_{UO_2}) at an electrochemical potential, E, is given by,

$$i_{UO_2} = nF(k')_{UO_2} A \exp[b_A(E - (E^e)_{A1}] \tag{9}$$

where b_A describes the relationship between current and potential and is termed the Tafel constant, and $(k')_{UO_2}$ is the chemical rate constant and an inherent property of the reaction (not to be confused with a kinetically obtained rate constant for a bimolecular homogeneous reaction between UO_2 and an oxidant), and $(E^e)_{A1}$ is the equilibrium potential. Here, the subscript $A1$ refers to one of the two possible anodic dissolution reactions, the dissolution of UO_2 as the uranyl ion. The second anodic reaction, $A2$, is the dissolution of the carbonate complexed uranyl ion (below). Writing this relationship in this form implicitly assumes that the applied electrochemical potential (E) is sufficiently positive of the equilibrium potential that the reverse reaction ($UO_2^{2+} + 2e^- \rightarrow UO_2$) cannot occur. This assumption will be maintained when writing similar relationships below. If the dependence of anodic dissolution rate on carbonate concentration is taken into account, then Eq. (9) is modified to read

$$i_{UO_2} = nF(k'')_{UO_2} A[CO_3]^m \exp[b'_A(E - (E^e)_{A2})] \tag{10}$$

where $[CO_3]$ is the total carbonate concentration and m is the reaction order with respect to total carbonate. The term $k''(UO_2)$ is the chemical rate constant for anodic dissolution as uranyl carbonate, b'_A is the Tafel constant for this reaction and E^e_{A2} is the equilibrium potential. It should be noted that not all surface sites are necessarily reactive and A could be modified to Af_A, where f_A is the fraction of the surface which is reactive. In chemical models this would commonly be termed the density of reactive surface sites, an entity implicitly included in the rate constants.

A similar relationship can be written for the cathodic half reaction ($H_2O_2 + 2e^- \rightarrow 2OH^-$).

$$i_{H_2O_2} = -nF(k)_{H_2O_2} A[H_2O_2]^p \exp[b_C(E - (E^e)_C)] \tag{11}$$

As for the anodic reaction, it is possible that not all surface sites can act as cathodic sites, or (as will be shown below for noble metal particles) some sites are preferential cathodes, and the surface area may need to be modified accordingly.

Generally, Eqs. (9)–(11) are written in the logarithmic form, e.g., for the anodic reaction,

$$\log(i_{UO_2}) = \log(nF(k')_{UO_2} A) + b_A(E - (E^e)_{A1}) \tag{12}$$

Plots of $\log(i)$ versus potential are termed Tafel plots. (A similar equation could be written for the cathodic reaction). When written in this form, the first term on the right hand side is recognizable as a chemical rate expression for the anodic half reaction, the second term accounting for the influence of potential. Extrapolating currents measured as a function of potential, E, to $E = E^e$ yields a value of the rate constant. At the equilibrium potential no measurable current flows since the forward reaction is dynamically balanced by the reverse reaction (e.g., $UO_2^{2+} + 2e^- \rightarrow UO_2$). The value of the current obtained by such an extrapolation of equations like (9)–(11) is commonly termed the exchange current, i_o. Inspection of the equations shows i_o is directly proportional to the rate constant and dependent on the concentrations of the species involved. The extrapolation of measured dissolution currents as a function of applied potential leading to the determination of i_o (Eq. (12)) is illustrated in Fig. 2.

As mentioned above, the corrosion potential (E_{CORR}), at which the corrosion reaction occurs, lies between the equilibrium potentials for the anodic and cathodic half reactions, and is the only potential at which the current for the anodic dissolution of UO_2 is equal, and opposite in sign, to the current for the cathodic reduction of H_2O_2. Thus, Eqs. (9)–(11) could be written in terms of $E - E_{CORR}$, rather than $E - E^e$, and extrapolation of their logarithmic form to E_{CORR} yields

$$\log(i_{UO_2}) = |\log(i_{H_2O_2})| = log(i_{CORR}) \tag{13}$$

where i_{CORR} is the corrosion current which can be converted to the corrosion rate in chemical units using Faraday's Law. This rate is the same as the oxidative dissolution rate determined in chemical kinetic studies. The relationship between E^e and E_{CORR}, and i^o and i_{CORR} according to Eq. (12) is illustrated in Fig. 2. Eq. (11) could also be written in the logarithmic form and measured currents for the cathodic reduction of H_2O_2 similarly extrapolated to $(E^e)_C$ and E_{CORR}.

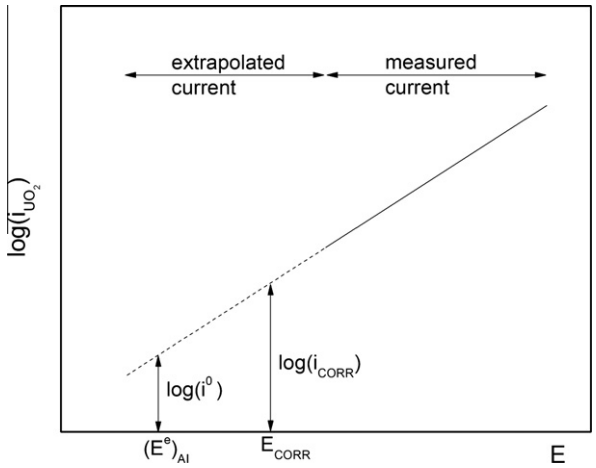

Fig. 2. Illustration of the extrapolation of measured anodic dissolution currents for UO_2, according to the Tafel relationship (Eq. (12)), to yield values of the exchange current, i_o, at the equilibrium potential, $(E^e)_{A1}$, and the corrosion current, i_{CORR}, at the corrosion potential, E_{CORR}.

In this second case, $(E^e)_C$ would be more negative than E_{CORR}, and the value of the current at E_{CORR} would also yield i_{CORR}.

2. Experimental studies

2.1. UO_2 oxidation

Since the steady-state oxidative dissolution of UO_2 proceeds through the pre-formation of UO_{2+x} [26], the kinetics of formation of this layer does not influence the overall oxidative dissolution kinetics providing the UO_2 surface is completely covered by this layer. Oxidation involves the injection of O^{2-} ions into vacant interstitial locations in the UO_2 cubic fluorite structure accompanied by the charge-balancing conversion of adjacent U^{IV} cations to U^V [3]. Based on corrosion potential (E_{CORR}) and charge-injection measurements it has been demonstrated that the rate of formation of this layer is ~200 times faster in H_2O_2 than in O_2-containing solutions of equivalent oxidant concentration [3]. However, as a measure of oxidation rate this approach can only be considered approximate, since the kinetics of surface oxidation (to UO_{2+x}) are difficult to separate from those of dissolution (as UO_2^{2+}).

In most kinetic studies of UO_2 oxidation and dissolution, the experiments are optimized to obtain dissolution rates rather than rate constants for oxidation or dissolution. This results in system specific rates dependent on the type of oxidant and its concentration, and the concentration of any UO_2^{2+} complexing agent. Applying these rates to systems where the conditions are different is not always possible, making it desirable to obtain rate constants for elementary reactions, since these are system-independent.

Rate constants have been determined in both chemical oxidative dissolution and electrochemical experiments [9,25,27,28]. Electrochemical rate constants were determined by the extrapolation of measured current–potential relationships as described in Section 1.3. In this manner rate constants for the anodic dissolution reaction, with and without carbonate complexation, and for the cathodic reaction (with Ox = H_2O_2 and O_2) were obtained. However, it should be emphasized that rate constants used in electrochemistry are fundamentally different from those used in chemical kinetics. Hence, direct comparison or interchange of rate constants between kinetic and electrochemical models are not possible.

Few second order rate constants have been reported [9,25]. In one paper, experimentally determined rate constants for oxidation of UO_2 by four different oxidants in aqueous solution with no UO_2^{2+} complexing agents are reported [25]. Older studies of UO_2 oxidation/dissolution by various oxidants did not always yield a rate constant [29]. The oxidants used in a more recent study [25] were $Fe(EDTA)^-$, H_2O_2, MnO_4^- and $IrCl_6^{2-}$. The logarithm of the rate constant was found to be linearly related to the one-electron reduction potential of the oxidant. This led to the conclusion that the rate determining step is the first electron transfer, and that the relationship between rate constant and redox potential enables the prediction of rate constants for other oxidants. That the first electron transfer step is rate-determining for H_2O_2 reduction is confirmed by electrochemical experiments, especially at lower $[H_2O_2]$ [30]. Molecular oxygen is also a potential radiolytical oxidant in a geological repository. As mentioned above, electrochemical studies indicate that H_2O_2 is approximately 200 times more reactive than O_2. This is in agreement with earlier observation by Hickey [31] that the corrosion rate in carbonate solution (pH = 9.8) is ~200 times faster in H_2O_2-containing than O_2-containing solution [31]. The relative reactivity estimated from the relationship between rate constant and one-electron reduction potential also gives a factor of 200 when comparing these two oxidants.

Since the rate determining step in oxidation of UO_2 is the first electron transfer, and both O_2 and H_2O_2 reduction involve multiple electron transfers, the oxidation of UO_2 by these oxidants will be a stepwise process, as demonstrated electrochemically [30,32]. For reasons discussed below, H_2O_2 is the most important oxidant in spent fuel dissolution, and the mechanism for UO_2 oxidation by H_2O_2 can be described by following reactions:

$$H_2O_2 + UO_2(s) \rightarrow OH^{\cdot} + OH^- + UO_2^+(s) \quad (14)$$

$$OH^{\cdot} + UO_2^+(s) \rightarrow OH^- + UO_2^{2+}(s) \quad (15)$$

The hydroxyl radical produced in the first step will initially be in the adsorbed state and being very reactive towards the UO_2 surface (the reaction is diffusion controlled), will inevitably react at the site of its formation [25].

The rate constants in Ref. [25] were determined in aqueous solutions containing no complexing agents when the kinetics of oxidant consumption could be influenced by the presence of surface deposits and, hence, is not solely governed by the redox process (even if the rate constants were determined from the initial slopes where the effect of dissolution is small). For this reason, the rate constants are not the true rate constants for oxidation. More recently, the kinetics of UO_2 oxidation by H_2O_2 was studied as a function of HCO_3^- concentration [9]. The second order rate constant increased linearly with HCO_3^- concentration over the range 0–1 mM, And for concentrations higher than 1 mM, became independent of the HCO_3^- concentration. This rate constant (7.3×10^{-8} m s^{-1}) is the dissolution-independent rate constant for the reaction between H_2O_2 and UO_2. In this reaction, only about 80% of the consumed H_2O_2 yields oxidative dissolution of UO_2 [33], the remaining 20% is presumed to be consumed by surface-catalyzed decomposition as will be discussed in more detail below.

$$2H_2O_2 \rightarrow O_2 + 2H_2O \quad (16)$$

It should be emphasized that the oxidation yield was determined for UO_2 powder, not pressed and sintered UO_2 pellets. Recent studies on UO_2 pellets show that a much larger fraction of H_2O_2 is catalytically decomposed on pellets [34].

For oxides which are more difficult to oxidize (compared to UO_2), the relative importance of surface-catalyzed decomposition of H_2O_2 is significantly higher. Experimental studies have shown that the activation energy for the oxide surface catalyzed decomposition of H_2O_2 seems to be independent of the type of oxide [22].

In aqueous solutions containing HCO_3^- and H_2O_2, peroxymonocarbonate (HCO_4^-) is formed, with redox properties similar to those of H_2O_2 itself [35]. The influence of ionic strength on the kinetics of the reaction between H_2O_2 and UO_2 has been studied [36], for solutions containing 0 and 10 mM HCO_3^-. At 0 mM HCO_3^-, the kinetics of H_2O_2 consumption is affected by dissolution of oxidized UO_2 while at 10 mM HCO_3^-, H_2O_2 consumption is completely governed by oxidation. The study clearly shows that the rate of oxidation (i.e. the rate constant at 10 mM HCO_3^-) is independent of the ionic strength, indicating the reactive oxidant is uncharged. Consequently, the reactive oxidant under these conditions is H_2O_2 rather than HCO_4^-. By contrast, a significant ionic strength effect was observed for a HCO_3^--free system, the kinetics of H_2O_2 consumption being strongly affected by dissolution of UO_{2+x}.

Oxidative UO_2 dissolution rates measured under various conditions (type of oxidant, oxidant concentration, HCO_3^- concentration and pH) have been reported [8,31,37–55]. In general, the oxidative dissolution rate increases with increasing oxidant and HCO_3^- concentrations. However, these trends are often not quantified in terms of rate constants, making their quantitative comparison difficult. Consequently, the rates have limited applicability.

Recently, the rate constants for HCO_3^--facilitated oxidative dissolution ($k = 1.7 \times 10^{-5}$ m s^{-1}) and for dissolution of oxidized UO_2 in pure water ($k = 7 \times 10^{-8}$ mol m^{-2} s^{-1}) were reported [9].

These rate constants were determined indirectly measurements of H_2O_2 consumption. The rate constants given above have been successfully employed in a comparison of the various dissolution rates reported in the literature [56]. Other authors have also reported rate constants for HCO_3^--facilitated oxidative dissolution of UO_2 ranging from 0.08 to 4.17 $mol^{-1}\,dm^3\,s^{-1}$ [8,57]. These rate constants were determined by fitting experimental data to a reaction mechanism involving several elementary reaction steps.

While the kinetics and mechanism of the oxidative dissolution of UO_2 can be considered fairly well understood, key issues remain to be resolved. Peroxide and carbonate have been shown to be coordinated in surface complexes, an indication that peroxide not only functions as an oxidant, but also influences the kinetics of the anodic dissolution reaction [58]. It has been proposed that an adsorbed U^V peroxycarbonate species is involved [58], but whether or not this will exert a significant influence at the lower peroxide and carbonate concentrations anticipated under waste repository conditions remains to be resolved.

One major unknown feature of the overall dissolution process is the complication introduced by the accumulation of corrosion product deposits on the UO_2 surface. Their key influence will be on the surface area available for dissolution and the redox conditions at exposed surface sites. Deposits would reduce the area exposed which will suppress dissolution. However, they also restrict the diffusive mass transport of species to (e.g., H_2 and Fe^{2+} produced by corrosion of the steel liner), and from (e.g., radiolytically-produced H_2O_2), the reactive surface. By confining H_2O_2 at, and inhibiting the flux of the redox scavengers to, the UO_2 surface, the dissolution rate could be sustained. Attempts to study these effects have been only partially successful [59]. The additional possibility that redeposited alpha emitters, released during fuel dissolution, will lead to a more complicated radiolysis scenario has been considered under the oxic conditions prevailing in the Yucca Mountain project [11] when the formation of oxidized deposits would be substantial.

Another important feature is the effect of in-reactor-induced alterations and aging on the reactivity of the solid phase, e.g. the effects of grain size, chemical composition, cracking and radiation-enhanced chemical reactivity.

2.2. Radiolysis effects

As noted above, water in contact with spent nuclear fuel will be irradiated by a mixed field of α, β and γ radiation. Whereas the β and γ activity decay to insignificant levels within 1000 years the α-activity persists for a much longer time period. Several studies have, therefore, focussed exclusively on the effect of α-radiolysis on the oxidation and dissolution of UO_2, using UO_2 pellets doped with α-emitters, irradiation of the UO_2/water interface with an external α-source, He^{2+} cyclotron irradiation of solutions containing nano-particles of UO_2 and irradiation of the UO_2 /water interface with high energy α-particles passing through the UO_2 disc. These are discussed below.

2.2.1. α-Doped UO_2

Gray [60] studied the leaching of ^{239}Pu and ^{238}Pu doped UO_2 pellets with specific activities of 1.06 and 172.6 MBq g^{-1}, respectively, in brine at 90 °C. The total uranium mass loss was found to be about one order of magnitude higher than from undoped pellets but not correlated to the specific α-activity of the doped pellets. Batch and sequential leaching have been carried out in demineralised water with monoliths [61] and crushed samples [62] of UO_2 doped with 0.1 and 10 wt.% $^{238}PuO_2$. The experimental data clearly demonstrated a significantly higher oxidative dissolution rate for the doped compared to un-doped UO_2 samples, but a clear correlation between rate and specific α-activity was not observed. The use of demineralised water leads to U(VI) release into the water accompanied by an increase in the U(VI)/U(IV) ratio on the UO_2 surface [63].

Stroes-Gascoyne et al. [64,65] have electrochemically, and in batch dissolution experiments, studied the effect of α-radiolysis on the oxidative dissolution of ^{238}Pu-doped UO_2 in 0.1 M $NaClO_4$ (pH 9.5) with and without 0.1 M carbonate. The oxidative dissolution rate was found to increase with increasing doping level, and, as can be expected, was lower in carbonate-free than in carbonate-containing solutions. An enrichment of ^{238}Pu on the UO_2 surface was observed in carbonate solutions.

Mennecart et al. [66] studied the dissolution of ^{225}Ac-doped nanoparticles of UO_2 under redox controlled reducing conditions (−800 mV/SHE) in 1 M NaCl at pH 6. The oxidative dissolution rate was found to increase with increasing specific alpha activity.

Rates from different studies are difficult to compare, since they are recorded under different geometric and chemical conditions. Experimental conditions for some published studies are given in Table 1 and the measured rates are plotted versus specific α-activity in Fig. 3 .

There is, in spite of considerable spread in the experimental data, a clear correlation between specific α-activity and oxidative dissolution rate, and the rates in solutions with 1 mM–0.1 M carbonate are 1–2 orders of magnitude higher than the rates in carbonate-free solutions. The lines in the figure illustrate the correlations for the carbonate and carbonate-free systems. This is consistent with electrochemically-measured rates in carbonate-free and carbonate-containing solutions [67].

2.2.2. Irradiation with external α-sources

Irradiation with alpha sources placed in water at various distances from the UO_2/water interface have been used in electrochemical studies [71], to demonstrate a clear influence of α-source strength on the surface-oxidation rate of UO_2 to UO_{2+x}, but not a clear dependence of oxidative dissolution rate on α-dose rate. The data was used in the assessment of spent fuel performance under proposed Canadian repository conditions [72], but it was acknowledged that their use was very approximate since no reliable and mechanistically justified function existed to fit, and hence extrapolate, the data. A more recent improved analysis of the data demonstrated that the corrosion potential (and, hence, the oxidative dissolution rate) was only dependent on α-dose rate at the lowest source strengths used [73]. At the higher source strengths, the UO_2 surface becomes redox buffered by the slow release (dissolution) of U^{VI} surface species into the carbonate-free solutions used. As a consequence, the full data set cannot be reliably used to predict, by extrapolation, the oxidative dissolution rates at lower dose rates.

Table 1
Experimental conditions for dissolution studies of alpha doped UO_2.

References	Chemical conditions	Material
[64,65]	0.1 M $NaClO_4$ (+0.1 M HCO_3^-), pH 9.5 deaerated	^{238}Pu doped pellets
[68]	Demineralised deaerated water	^{238}Pu, ^{239}Pu doped pellets
[69]	Ar (0.02% CO_2)) equilibrated water.	^{233}U doped pellets
		^{238}Pu doped pellets
	N_2 equilibrated MQ-water[a]	
[70]	1 mM HCO_3^-, Ar – equilibrated	$^{238/239}Pu$ doped pellets
[66]	1 M NaCl, pH 6, −800 mV (SHE)[b]	^{225}Ac doped nanoparticles

[a] Water with a resistivity of 18.2 Mohm cm-1 prepared using Milli-Q-plus ion exchange columns.
[b] Standard hydrogen electrode.

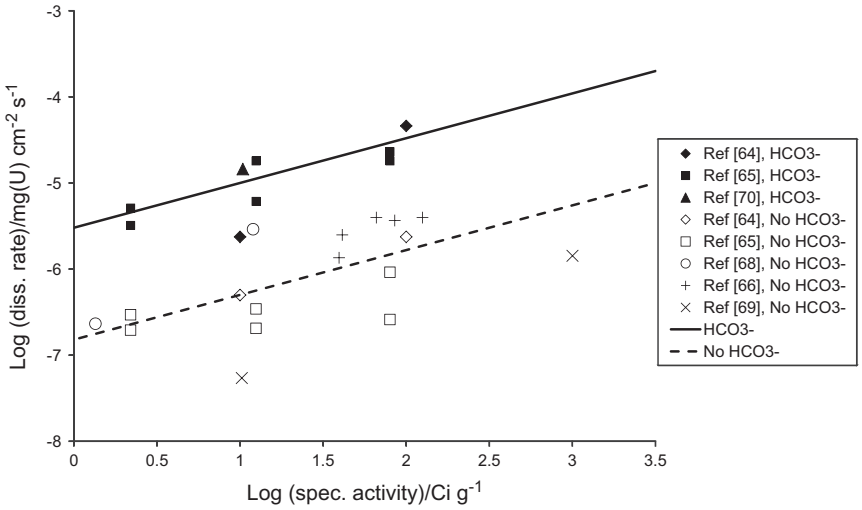

Fig. 3. Dissolution rate for α-doped UO_2 plotted as a function of specific α-activity. The straight lines have been included (not fitted) to enable comparison between systems containing HCO_3^- and systems without HCO_3^-.

Sattonay et al. [74] used a cyclotron to irradiate the UO_2/water interface with a high energy (45 MeV) beam of $^4He^{2+}$ ions (α particles). The $^4He^{2+}$ ions passed through a thin (<300 μm) UO_2 disc emerged into aerated deionised water with an energy of ≈5 MeV, which is comparable to the maximum energy of α-particles emitted from spent fuel.

In aerated deionised water, the rate of uranium dissolution was found to depend on the $^4He^{2+}$ flux increasing by four orders of magnitude for the highest flux (3.3×10^{11} $^4He^{2+}$ cm^{-2} s^{-1}) compared to zero flux. The secondary phase, metastudtite ($UO_4 \cdot 2H_2O$), was found on the UO_2 surface, due to the build up of high H_2O_2 concentrations at the UO_2 surface. The relevance of these measurements to repository conditions is limited due to the very high α-fluxes used and high H_2O_2 concentration (3.5 mM) achieved. Suzuki et al. [75] studied the oxidation and dissolution of UO_2 colloids in carbonate-rich solutions irradiated with $^4He^{2+}$ ions from a cyclotron. The experimental data are consistent with the generally accepted mechanism involving two sequential reaction steps: oxidation of the UO_2 surface by H_2O_2 followed by dissolution of the oxidized surface species. As the carbonate concentration was increased the oxidative dissolution rate reached the consumption rate of H_2O_2. Loss of H_2O_2 by catalytic decomposition to O_2 and H_2O at the UO_2 surface was, contrary to suggestions and observations in other publications [33], not observed.

2.2.3. Mixed radiation field

Corrosion potential (E_{corr}) time plots recorded on various used fuel specimens exposed to aerated 0.1 M $NaClO_4$ solutions (pH 9)) are given in [3], The characteristics of the fuel used to construct the electrodes and the (approximate) steady state E_{corr} values eventually achieved are given in Table 2. The steady state E_{corr} increases with β + γ dose rate, indicating a dependence of oxidative dissolution rate on dose rate.

Jegou et al. [76] performed leaching and oxidative dissolution experiments on polished discs of $^{(238/239)}$Pu-doped UO_2 and spent fuel fragments in the absence and presence of an external gamma irradiation source. The radiation dose rates are given in Table 3 along with the approximate distances the particular type of radiation travelled in the experiment.

The experiments were performed in deionised water (i.e., HCO_3^- free solution) and the uranium concentration in solution determined after acidification. The H_2O_2 concentration was also measured in the experiments.

The experimental results are given in Table 4.

The effects of mixed radiation fields and purge gas are very clear in the data of Jegou et al. [76]. In Ar-saturated solution the rate of oxidative dissolution increased by a factor 10–30 on γ-irradiation, due to an increase in the steady state H_2O_2 concentration by a factor of 1.5–10 in the γ-irradiated volume. In air-saturated solutions e_{aq}^- and $H^\cdot$ are effectively scavenged by O_2,

$$e_{aq}^- + O_2 \rightarrow O_2^- \quad (17)$$

$$H + O_2 \rightarrow HO_2 \quad (18)$$

$$HO_2 = O_2^- + H^+ \quad (19)$$

$$2HO_2 \rightarrow H_2O_2 + O_2 \quad (20)$$

leading to an increase in steady-state H_2O_2 concentration by $\sim 10^3$ compared to an anoxic system. As a consequence, the oxidative dissolution rate increased by several orders of magnitude. Such an increase in the steady state H_2O_2 concentration with increasing β and γ dose rates would account for the corrosion potential increases observed by Shoesmith [3] and is also in qualitative agreement with the results of Jegou et al. [76].

2.3. Simfuel

A complex array of changes occurs within the fuel matrix as a consequence of in-reactor fission. These physical and chemical

Table 2
Characteristics of fuel and measured steady state corrosion potentials [3].

Fuel	Dose rates (Gy h^{-1})			E_{corr} (mV versus SCE)
	α	β	γ	
Darlington L23139C	33.1	7734	260.6	340
Pickering PA07993 W	15.0	125.3	401.3	280
Bruce BF21271C	160.9	507.1	31.4	31.4

Table 3
Dose rates (Gy h^{-1}) for the spent fuel and α-doped fuel under external γ-irradiation [76].

Radiation	Spent fuel	α-doped UO_2
α (40 μm)	1600	110
β (300–400 μm)	2300	
γ (entire volume)	650	650

Table 4
Leaching data from Jegou et al. [76].

Solid	Dissolution rate (mg m^{-2} d^{-1})		Dissolution rate (mg $m^{-2}d^{-1}$)	Dissolution rate (mg $m^{-2}d^{-1}$)	H_2O_2 (M)	
	Air	Ar	γ-Radiation, air	γ-Radiation, Ar(4% H_2)	Air	Ar
Doped UO_2	0.5	0.2			ND[b]	$<2 \times 10^{-8}$
R(U)[a]			83	6	1.2×10^{-4}	3×10^{-8}
Spent fuel	0.4				$<4 \times 10^{-6}$	
R(U)[a]			34	6.5	1.2×10^{-4}	2×10^{-7}
R(^{134}Cs)[a]			312	27		
R(Sr)[a]			295	<40		

[a] R(X): Dissolution rate based on the element or nuclide X.
[b] ND: Not determined.

changes have been investigated in detail [77–79], and recently summarized [80,81]. While the physical changes, such as the introduction of fission gas porosity, and the generation of the pellet rim structure [82], cannot be reproduced in non-radioactive analogues of spent UO_2, the key chemical changes have been simulated in SIMFUELs [83–85]. SIMFUELs are UO_2 pellets doped with non-radioactive elements (Ba, Ce, La, Mo, Sr, Y, Zr, Pd, Rh, Ru, Nd) to replicate the chemical effects of in-reactor burn-up. The key features of these materials which are most likely to influence UO_2 reactivity are; (i) the trivalent rare earth elements (RE^{3+}) which act as dopants in the U^{IV} oxide structure and lead to an increase in electrical conductivity [86–88] and (ii) the noble-metal dopants (Pd, Ru, Rh, Mo) which are unstable in the oxide matrix and segregate to form noble-metal particles, commonly referred to as ε-particles. Primarily, to date, these materials have been used in electrochemical experiments to elucidate the mechanisms of oxidant (O_2, H_2O_2) and reductant (H_2) reactions, and how they are influenced by these changes in chemical properties.

Comparison of oxidative dissolution experiments conducted on SIMFUELs, UO_2 and spent fuel, have proven inconclusive, primarily because no common sample preparation and experimental procedure was used [89]. Qualitatively, oxidative dissolution rates of SIMFUELs appeared lower than those of UO_2. Recent electrochemical experiments suggest that the reactivity of UO_2 is decreased at high simulated burn-up [81], a trend also seen in spent fuel dissolution experiments [90,91]. A similar influence of burn-up on the air oxidation of SIMFUEL and spent fuel has also been observed [92–94]. These last studies show that doping changes the reaction pathway, but a mechanistic similarity air oxidation and fuel oxidative dissolution remains to be demonstrated. To date, no study of the influence of irradiation on such doped materials has been performed. A very recent experimental study reveals that radiation-induced dissolution of SIMFUEL is considerably slower than for pure UO_2 [34]. This is partly attributed to differences in the reactivity of H_2O_2 towards these materials. For SIMFUEL, a much larger fraction of the H_2O_2 undergoes catalytic decomposition than in the case of pure UO_2.

2.4. H_2 effect on fuel and UO_2 dissolution

A key processes inside a failed waste container will be the corrosion of carbon steel to produce the potential oxidant scavengers Fe^{2+} and H_2

$$Fe + 2H_2O \rightarrow Fe^{2+} + H_2 + 2OH^- \quad (21)$$

$$3Fe + 4H_2O \rightarrow Fe_3O_4 + 4H_2 \quad (22)$$

Since H_2 pressures up to 5 MPa are expected to develop as a consequence in a sealed repository [69,95], a considerable effort has been expended to determine the effect of H_2 on dissolution of spent fuels, fuel specimens doped with alpha emitters, SIMFUELs, and UO_2 pellets and powder (sometimes containing the noble metal, Pd).

Many of these studies on spent fuel have been recently summarized [69,80,95] and reinforce the observations in other studies [96–99]. The key observations are: (i) the dissolved U levels were well below the solubilities of any U^{VI} solids that could feasibly form in the solutions used. Comparison to calculated UO_2 solubilities indicate this is the only phase that could equilibrate with the solution at these concentrations. (ii) the concentrations of radiolytically-produced O_2 was commonly around or below the analytical detection limit of 10^{-8} mol dm^{-3}. At the low temperatures employed, reaction between O_2 and H_2 would not be expected in the absence of catalysis by the UO_2 surface. (iii) The concentrations of redox sensitive radionuclides decreased throughout the experiments. Even when complete suppression was not observed (for PWR specimens with a burn-up of 40 MWd/kg), gas and solution analyses indicated suppressed steady-state conditions for radiolytically-formed oxidants (400–900 days) and dissolved actinides and fission products, indicating inhibited fuel dissolution [100].

These, and additional experiments on α-doped UO_2 [80,95], show that even small amounts of dissolved H_2 ($\leqslant 10^{-4}$ mol dm^{-3}) are sufficient to suppress the U release rate to effectively immeasurable levels. In addition, X-ray photoelectron spectroscopy was used to demonstrate that the surface of a 10% ^{233}U-doped UO_2 remained unoxidized over the full exposure period (>2.2 years) [80]. It is clear from these studies that dissolved H_2 can suppress the oxidative dissolution of fuel and reduce the concentrations of both radiolytic-oxidants and redox-sensitive radionuclides. To act as a reductant H_2 must be activated (i.e., dissociated into reactive H atoms) since it is unlikely to be reactive in homogeneous solution at the temperatures and H_2 concentrations reported.

A dramatic effect of H_2 was observed on UO_2 electrodes in γ-irradiated 0.1 mol dm^{-3} NaCl (pH = 9.5) solutions pressurized with H_2 to 5 MPa (equivalent to $\sim 4 \times 10^{-2}$ mol dm^{-3} of dissolved H_2). The corrosion potentials were considerably lower than in Ar-purged solutions, and achieved values that approached the reversible potential for the reaction

$$H_2 \leftrightarrow 2H^+ + 2e^- \quad (23)$$

Slow changes in the corrosion potential with time suggested that the state of the UO_2 surface was slowly changing. It was claimed, but not proven, that γ-radiolysis induced decomposition of H_2 to produce adsorbed $H^\cdot$ radicals leading to reduction of the UO_2 surface. These changes appeared to be at least partially irreversible since the corrosion potential did not fully recover to the value expected in Ar-purged solutions when the H_2 pressure was removed [101,102].

Since noble metals are well known catalysts for oxidation/reduction reactions, especially the $H_2/H^\cdot/H^+$ reaction, and three of the four predominant components of the ε-particles (Rh, Pd, Ru)

are especially good catalysts for this reaction [103], one would expect H_2 to be activated on the surface of noble metal particles in SIMFUEL or spent fuel. Since the noble metal (ε) particles are galvanically coupled to the rare earth-doped UO_2 in SIMFUEL and spent fuel, this introduces the possibility that H· atoms adsorbed on the noble metal particles could act as reductants. Using electrochemical and surface analytical methods, Broczkowski et al. showed that this was indeed the case [104]. The corrosion potential decreased in proportion to the degree of simulated burn-up (i.e., the number density and size of available particles) and the pressure of H_2. For either a sufficient number density of particles or a sufficiently high H_2 pressure, the corrosion potential of the SIMFUEL was suppressed to values below the thermodynamic threshold for UO_2 oxidation, confirming suppression of UO_2 oxidation.

Recent kinetic studies [105] have demonstrated that the recombination reaction between H_2O_2 and H_2 is catalyzed on Pd-particles at a diffusion-controlled rate. Also, experimental studies on the catalytic effects of 0–3% Pd inclusions on the H_2O_2-induced dissolution of UO_2 as a function of H_2 pressure in HCO_3^--containing solutions [106] showed the inclusions could either catalyze oxidation or reduction of the UO_2 surface. These results are consistent with the results of experiments conducted on SIMFUELS which showed the oxidation of the UO_2 surface in H_2O_2-containing solutions could be prevented or reversed in the presence of a sufficient concentration of dissolved H_2 [104]. However, the work by Trummer et al. [106] provided the kinetic data essential for incorporating the mechanism for noble metal catalyzed reduction of the UO_2 surface into a kinetic model. When the mechanism for noble metal catalyzed reduction of the UO_2 surface is included in simulations of time resolved and long-term experiments on spent fuel dissolution in 10 mM HCO_3^- solution [107], the experimental data can be reproduced quite well, giving further support for the proposed mechanism. The mechanism is illustrated in Fig. 4.

While the catalytic influence of ε-particles offers an explanation for the ability of H_2 to suppress spent fuel and SIMFUEL oxidative dissolution it cannot explain the suppression of the oxidative dissolution of α-doped UO_2, when these particles are absent. Pastina and LaVerne [108] studied the effect of H_2 on radiolytic production of H_2O_2 using $^4He^{2+}$ from an accelerator. In contrast to the observations made using α-doped pellets, no significant H_2 effect was observed, although a numerical simulation indicated a strong H_2 effect should have been present. This contradiction has been subsequently resolved in recent studies showing that the influence of H_2 on the α-radiolytic production of oxidants is, in fact, strongly dependent on the dose rate [109]. In the simulation of Pastina and LaVerne, the α-energy was distributed throughout the whole cell volume whereas the α-energy is, in fact, deposited in a very small volume limited by the maximum range of the α-particles in water. Consequently, the dose rate used in their simulation was several orders of magnitude lower than the actual dose rate in the experiment. When this limitation in deposition volume is accounted for [109], the simulation reproduces the experimental results. However, the radiolytic H_2 effect is not sufficient to completely stop oxidative dissolution. For spent nuclear fuel, the catalytic H_2 effect will dominate since it is effective at much lower H_2 concentrations than the radiolytic H_2 effect.

Since most α-decays are accompanied by the emission of γ-photons, α-doped UO_2 is not only a source of α-radiation. While the γ-dose rate is significantly lower than the α-dose rate, the volume affected by γ-radiolysis is considerably larger. Furthermore, the *G*-values for radical production are much higher for β- and γ-radiolysis than for α-radiolysis. The reducing radicals formed in a β- or γ-irradiated solution containing H_2 are capable of reducing redox sensitive radionuclides (e.g., U(VI)). As demonstrated by Trummer and Jonsson [109], the impact of H_2 in combination with low γ-dose rates on dissolved U(VI) is expected to be considerable. This is a plausible explanation of the H_2-effect observed in several studies using α-doped UO_2.

3. Modelling radiolysis effects on spent nuclear fuel dissolution

As stated above, spent nuclear fuel contains α, β and γ emitting radionuclides. Water in contact with the fuel surface will, therefore, unavoidably be radiolysed by a field of mixed radiation producing both molecular and radical oxidants (H_2O_2, OH, HO_2) and reductants (H_2, e^-_{aq}, H). The rate of radiolytic production of the different species depends on their radiation chemical yields (*G*-values) the composition of the radiation field and the overall dose rate, and is given by the equation.

$$\frac{d[X]}{dt} = \left(G_\alpha(X)\,\dot{D}_\alpha + G_\beta(X)\,\dot{D}_\beta + G_\gamma(X)\,\dot{D}_\gamma\right)\rho \tag{24}$$

where [*X*] is the concentration (*M*), $\dot{D}$ is the dose rate in J kg^{-1} s^{-1}, *G*(*X*) the primary yield (mol J^{-1}) and ρ is the fluid density (the subscript indicates radiation type).

3.1. Dose rates

A key feature of all radiolytic models for fuel corrosion is the deposition of radiation energy into water leading to the formation of radiolytic oxidants. Two distinctly different approaches have been employed; one in which the radiation dose rate-distance profile is calculated, and a second in which the radiation energy is assumed to be uniformly deposited within a layer of specified thickness. This second approach is commonly adopted with alpha

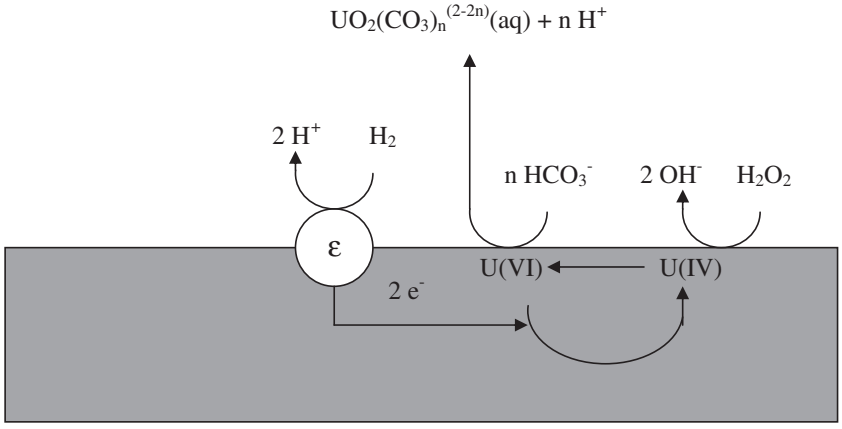

Fig. 4. Elementary processes involved in radiation induced oxidative dissolution of spent nuclear fuel.

radiation when it is easier to specify an average deposition range for the α-particle in water.

The spatial distribution of dose rates for the emitted α, β and γ radiation fields can be calculated from the radionuclide inventory of the spent fuel. Garisto [110] calculated the energy spectrum of α-particles emitted from used CANDU™ fuel. The energy absorption in water layers at different distances from the surface was calculated taking into account the energy and direction of the emitted particle. The maximum range of the emitted α-particle is given as 34.4 μm but 90% of the α-energy was found to be absorbed within 18 μm of the fuel surface. Spatial distributions of α and β dose rates in water in contact with 38 and 55 MWd/kg fuel burn up have been calculated by Cera et al. [100] and Nielsen and Jonsson [111], taking into account the radionuclide inventory, isotropic emission of radiation, and fuel self shielding. In agreement with Garisto [110], the α-dose rate was found to decrease sharply with distance from the fuel/water interface. A similar spatial dose distribution is indicated but not quantified, in a recent publication by Poulesquen and Jegou [112].

The spatial β-dose rate distribution displays a sharp decrease within a distance of 1 mm [100,111] from the fuel surface and then exhibits a long tail out to a range of 3.5 mm from the fuel surface.

Poinssot et al. [95] calculated the α- energy absorbed by water in contact with the fuel surface using the equation

$$\frac{dE}{dt} = \frac{1}{\eta}\overline{E}_{\alpha}A_{v}\cdot S\cdot L \tag{25}$$

where $\overline{E}_{\alpha}$ is the average α-decay energy, A_v is the activity per unit mass, S is the surface area, L is the α-range in the fuel matrix, and η is a geometric factor giving the fraction of α-particles reaching the water phase. Energy loss in the solid phase is not taken into account.

A thin layer of water in contact with the fuel surface, whose thickness is determined by the mean penetration depth of the α-particles in water (approx. 45 μm), is assumed to be uniformly irradiated. Note the mean penetration depth used in [95] is different from that used in [110]. This method of dose rate calculation gives no detailed information on the spatial dose distribution close to the fuel/water interface. Similar models for dose calculations have been used by Liu and Neretnieks [113] and Shoesmith et al. [114], although subsequent versions of the latter electrochemical approach did account for the spatial dependence of the α dose rate [115].

3.2. G-values

The primary G-values for α, β and γ radiation are fairly well known and the primary yield of hydrogen peroxide (the dominant oxidant) is only slightly reduced by radical spur reactions with scavengers for $<10^7(s^{-1})$, the scavenging capacities for e^-_{aq} and OH being defined as the product of the scavenger concentration and the appropriate rate constant [116–118].

3.3. Oxidative dissolution mechanism

The reaction mechanism for the oxidative dissolution of the fuel matrix is given by reactions (3) and (4) above.

The total rate of oxidation of the fuel surface is given by Eq. (26)

$$\frac{dUO_2^{2+}(s)}{dt} = A_{UO_2}\sum_{Ox=1}^{n} k_{Ox}[OX]\frac{n}{2} \tag{26}$$

for a chemically-based model, where A_{UO_2} is the surface area of solid UO_2, n is the number of electrons in the redox process, k_{OX} the interfacial rate constant for a given oxidant and [OX] is the oxidant concentration adjacent to the fuel/water interface. The dissolution (reaction (4)) is enhanced in solutions containing $UO_2^{2+}(aq)$ complexing agents (e.g. HCO_3^-) in groundwaters.

In an electrochemical model, the rate of UO_2 dissolution will be given by Eq. (9) modified to Eq. (11) if dissolution is accelerated in carbonate-containing solutions. In this case, the potential is determined from the oxidant concentration which is calculated from the radiolytic production.

3.4. Oxidation of the fuel matrix by radiolytic oxidants

The development of a radiolytic model for fuel dissolution requires the consideration of radiolytic oxidant production, homogeneous reactions in aqueous solution, diffusive transport and heterogeneous reactions on the fuel surface. Interfacial rate constants can be obtained in batch or flow experiments by measuring the oxidant consumption and/or uranium concentration as a function of time, or in electrochemical experiments by measuring electrochemical currents for the anodic and cathodic reactions. A review of rate constants for $UO_2(s)$ and radical and molecular oxidants is given by Roth and Jonsson [56] and for electrochemical reactions by King and Kolar [119].

Poinssot et al. [95], using a matrix alteration model (MAM), modelled oxidation and dissolution based on a number of assumptions including uniform α-irradiation of a 45 μm thick water layer, and the assumption that half of the oxidants reached and reacted quantitatively with the fuel surface. This approach cannot be considered kinetically-based.

A kinetic model describing water radiolysis, oxidative dissolution and allowing for diffusion of radiolytic oxidants away from the UO_2 surface was developed by Christensen et al. [120], Christensen [121], and a similar approach was adopted by Kelm and Bonert [122], Lundström [123] and Poulesquen and Jegou [112]. In the absence of information on the kinetics of the heterogeneous reactions between the UO_2 surface and radiolytic oxidants, it was assumed, based on a reaction scheme originally proposed by Christensen and Bjergbakke [124], that the heterogeneous reactions could be mimicked by assuming they would be similar to those expected to occur in homogeneous solution. This required the arbitrary assumption that a monolayer of the UO_2 surface reacted as if it were dissolved in a thin layer of water near the UO_2 surface. Since, even for homogeneous solutions, no kinetic constants for the reaction of U species with radiolytic species existed, rate constants available for the reaction of other dissolved metallic species were adopted. Subsequently, an attempt to readjust these constants, based on the mechanism of UO_2 oxidation and dissolution determined electrochemically, was made [120].

Model calculations were performed using MAKSIMA-CHEMIST [125] and compared with the results of electrochemical experiments, and reasonable agreement between measured and calculated corrosion rates achieved [120]. This arbitrary fitting process is subject to many uncertainties, including an incomplete understanding of the UO_2 oxidation and dissolution mechanism at the time the model was developed.

In the model of Christensen et al. [120] the rate-determining reactions and rate constants for oxidation by OH, H_2O_2 and O_2 are given by

$$OH + UO_2 = UO_3H \quad k = 4\times 10^8\ (\text{dm3 mol}^{-1}\ \text{s}^{-1}) \tag{27}$$

$$H_2O_2 + UO_2 = UO_3H + OH$$
$$k = 2\times 10^{-1}\ (1998\ \text{adjusted to}\ 2\times 10^{-2})\ (\text{dm}^3\ \text{mol}^{-1}\ \text{s}^{-1}) \tag{28}$$

$$O_2 + UO_2 = UO_3H + HO_2 - H_2O$$
$$k = 1\times 10^{-3}\ (\text{dm}^3\ \text{mol}^{-1}\ \text{s}^{-1}) \tag{29}$$

These homogeneous rate constants k_H $(\text{mol dm}^{-3})^{-1}\,\text{s}^{-1}$ can be converted to surface-based rate constants k_S (m s^{-1}) using the equation

$$k_S \times \frac{A}{V} = k_H \times C(UO_2) \tag{30}$$

in which A is the surface area (m^2), V is the volume (m^3) and $C(UO_2)$ is the concentration (mol dm^{-3}) corresponding to a dissolved monolayer. The resulting rate constants are compared to experimentally determined interfacial rate constants in Table 5.

The rate constants for the radical oxidants HO_2 and O_2^- were set to 2×10^8 $(\text{mol dm}^{-3})^{-1}\,\text{s}^{-1}$ (corresponding to 2.5 m s^{-1}). It is evident that the rate constants used by Christensen et al. [120] grossly overestimate the reactivity of the radical species and underestimate the reactivity of the molecular species. The interfacial rate constant (k_S) for the OH reaction is five orders of magnitude higher than the diffusion-limited rate constant for this type of heterogeneous reaction. This overestimate can be partially explained based on later studies, which showed that the corrosion potentials observed in the experiments used to determine rate constants in this model were predominantly determined by changes in pH at the fuel surface (caused by rapid hydrolysis of dissolved uranyl ions) rather than a dependence on gamma dose rate. Failure to acknowledge the diffusion limit then leads to the adoption of an unrealistic value.

3.5. Relative impact of radiolytic oxidants

A kinetic analysis of the system where the individual rates of oxidation for each oxidant are compared shows H_2O_2 to be the most important [128]. Individual rates depend on both the rate constant and oxidant concentration ($r = k[\text{Ox}]$). Consequently, while the radical oxidants such as $OH^{\cdot}$ and $CO_3^{\cdot-}$, have very high rate constants (diffusion limited), the surface concentrations will never reach sufficiently high levels to compete with the molecular oxidants H_2O_2 and O_2. Also, since the reactivity of H_2O_2 with UO_2(s) is about 200 times higher than that of O_2, an O_2 concentration 200 times higher than the H_2O_2 concentration would be required to achieve comparable rates. However, it should be stressed that the original assessment of the relative impact of radiolytic oxidants was based on data for UO_2 powder suspensions. Under these conditions, approximately 80% of the H_2O_2 yields oxidative dissolution of UO_2. The remaining 20% is assumed to undergo catalytic decomposition on the UO_2 surface producing H_2O and O_2 [33].

H_2O_2 decomposition has been shown to be possible on UO_2 surfaces [29,129], and evidence exists to show it will be catalyzed on a UO_{2+x} surface containing a mixture of U^{IV} and U^{V} oxidation states [3,130]. Other studies have shown that the activation energy for oxidation of UO_2(s) depends on the UO_2 particle size (increases with decreasing size) [131,132]. Studies on the catalytic decomposition of H_2O_2 on metal oxide surfaces in general have not revealed any particle size effects on the activation energy [22]. Consequently, the fraction of H_2O_2 undergoing catalytic decomposition is expected to increase with decreasing particle (or grain) size. As a result, the relative impact of the radiolytic oxidants can change with the characteristics of the solid UO_2 phase.

An additional issue is the effect of noble metal (ε) particles. These particles will change the relative kinetics of UO_2 corrosion supported by O_2 and H_2O_2 reduction. Electrochemical studies [59] show that O_2 reduction is significantly catalyzed in the presence of noble metal particles whereas their influence on H_2O_2 reduction is much harder to detect. This is argued to be a consequence of the ability of H_2O_2 to rapidly create its own catalytic sites (U^{IV}/U^{V} donor–acceptor sites) on the UO_2 surface which makes the kinetics of H_2O_2 reduction on UO_2 and the noble metal particles only marginally different [59]. A schematic representation of this mechanistic difference, which leads to similar rate constants for the reduction of both oxidants, is shown in Fig. 5.

An attempt to account for this influence of noble metal particles was incorporated into the electrochemical model [114,119], although, in the absence of H_2O_2 decomposition, it made little difference to the predicted dissolution rates. More recently, Trummer et al. have experimentally demonstrated that H_2O_2 reduction is catalyzed on noble metal particles and a reconsideration of the kinetics of H_2O_2 and O_2 reduction is merited [133]. It is important to keep in mind that even though the rate constants are similar for the oxidation of UO_2 by H_2O_2 and O_2 catalyzed by noble-metal particles, the overall oxidation of UO_2 is a combination of catalyzed and un-catalyzed oxidation. Due to the fairly low surface concentrations of noble metal particles, the overall rates of oxidation by H_2O_2 and O_2 are still different to each other. Trummer et al. recently showed that the impact of H_2O_2 is only marginally decreased and that the impact of O_2 is increased from 1% to 3% taking the noble metal inclusion catalytic effect on H_2O_2 and O_2 reduction into account [133].

The possibility of catalytic decomposition of H_2O_2 was incorporated into the model of Christensen et al. [120] by arbitrarily specifying the thermal decomposition mechanism of H_2O_2 as the rate determining step

$$H_2O_2 \rightarrow O + H_2O \quad k = 10^{-3}\ \text{s}^{-1} \tag{31}$$

$$O + O \rightarrow O_2 \quad k = 10^{9}\ \text{dm}^3\ \text{mol}^{-1}\ \text{s}^{-1} \tag{32}$$

While these rate constants as well as the reaction mechanism were arbitrarily chosen, they were consistent with the kinetics established experimentally for the reaction of H_2O_2 on UO_2, for H_2O_2 concentrations in the range $\sim 10^{-5}$ mol dm^{-3} to 10^{-2} mol dm^{-3} [134]. Within this range, it was argued that rapid H_2O_2

Table 5
Interfacial rate constants for reactions between UO_2(s) and aqueous oxidants.

Oxidant	k (m s^{-1})	Refs.
OH	1.7×10^{-5}	[25]
OH	5	[120]
H_2O_2	1.3×10^{-8}	[25]
H_2O_2	7.3×10^{-8}	[9]
H_2O_2	2.5×10^{-9}	[120]
H_2O_2	2.5×10^{-10}	[121]
H_2O_2	1.8×10^{-7}	[126]
H_2O_2	2.0×10^{-8}	[40]
H_2O_2	6.0×10^{-7}	[127]
O_2	3.6×10^{-10}	[128]
O_2	3.6×10^{-10}	[8]
O_2	$\approx 3 \times 10^{-9}$	[39]
O_2	1.25×10^{-11}	[120]

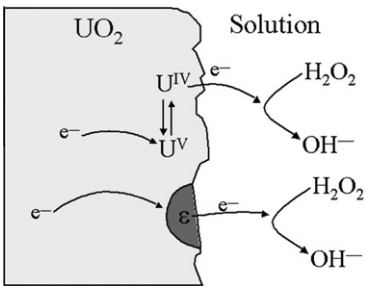

Fig. 5. Schematic illustration showing H_2O_2 reduction on noble metal (ε-particles) and on the UO_2 surface preoxidized by H_2O_2 to create donor (U^{IV}) – acceptor (U^{V}) sites.

decomposition to yield the slower corrosive oxidant O_2 could explain the independence of the corrosion potential on H_2O_2 concentration. To account for this, the rate of H_2O_2 decomposition was made greater than its rate of reaction with UO_2, thereby ensuring that UO_2 corrosion was primarily driven by reaction with O_2. Subsequently, this mechanism of fast decomposition followed by slow reaction of O_2 with UO_2 was shown to explain the corrosion potential behaviour in the presence of H_2O_2 produced by external alpha-radiation sources [73]. However, it was acknowledged by Christensen et al. [120] that their model could not account for the potential dependence of rate constants for the key reactions, critical to determining their relative importance outside the experimental range of H_2O_2 concentrations used to establish the model.

A re-evaluation of the consequences of H_2O_2 decomposition was undertaken by Shoesmith et al. [114] and King and Kolar [119]. In this model, based on electrochemical principles, the potential dependence of individual rate constants is accounted for. Based on electrochemical data, the following rate constants for the half-cell reactions were adopted for the key H_2O_2 and O_2 surface reactions involved in UO_2 (spent nuclear fuel) corrosion and H_2O_2 decomposition

$$H_2O_2 \rightarrow O_2 + 2H^+ + 2e^- \quad k = 7.4 \times 10^{-6}\ \text{cm s}^{-1} \tag{33}$$

$$H_2O_2 + 2e^- \rightarrow 2OH^- \quad k = 1.2 \times 10^{-10}\ \text{cm s}^{-1} \tag{34}$$

$$O_2 + 2H_2O + 4e^- \rightarrow 4OH^- \quad k = 1.4 \times 10^{-10}\ \text{cm s}^{-1} \tag{35}$$

The similarity in rate constants for H_2O_2 and O_2 reduction reflect the fact that O_2 reduction was observed to be strongly catalyzed by the presence of noble metal particles in the SIMFUEL used to generate the experimental database whereas any catalytic effect of these particles on H_2O_2 reduction was experimentally difficult to detect. This is argued to be a consequence of the ability of H_2O_2 to rapidly create its own catalytic sites (U^{IV}/U^{V} donor–acceptor sites) on the UO_2 surface which makes the kinetics of H_2O_2 reduction on UO_2 and the noble metal particles only marginally different. A schematic representation of this mechanism is shown in Fig. 4.

Despite this increased rate constant for O_2 reduction the model predicts that >99% of the radiolytically-produced H_2O_2 would lead to UO_2 corrosion and hence that H_2O_2 decomposition would be insignificant. This is because, even at its most positive (i.e., for relatively fresh spent nuclear fuel when alpha radiation dose rates are highest) the corrosion potential remains too negative to support H_2O_2 oxidation, the anodic half reaction of the overall H_2O_2 decomposition reaction.

In kinetic modelling, the fraction of H_2O_2 undergoing catalytic decomposition and the influence of noble-metal particles can be accounted for if the fuel characteristics are known.

3.6. Accounting for the spatial dose distribution

Publications on simulations of radiation-induced oxidation of spent nuclear fuel based on the spatial dose rate distribution are scarce [107,112,121,123,135,136].

Christensen [121] used a three compartment model and included Ficks 1st law

$$F = A \times D \times \frac{dC}{dx} \tag{36}$$

where F denotes flow, D is the diffusion constant, C is the concentration and x is distance. It should be noted that this approach is valid only at steady-state conditions. Results from oxidative dissolution and radionuclide leaching experiments in Karlsruhe [137] with 6.4 g spent fuel with 4.2 cm^2 geometric surface area in 200 cm^3 distilled water and 250 cm^3 gas phase (Ar) were used in the simulations. The compartments used in the calculations are given in Table 6.

Lundström [123] improved the model by increasing the number of compartments and using Ficks second law $\frac{dC}{dt} = D\frac{d^2C}{dx^2}$ where C is the concentration, D is the diffusion constant, t is the time and x is the compartment length.

Radiolysis calculations are carried out in each compartment for each chosen time step and then diffusion between the compartments takes place during the same time step. The thickness of the first compartment was 30 μm, thus the α-dose rate was not spatially resolved in the calculations by Lundström et al.

3.7. Model applications

Maksima Chemist and the reaction scheme given by Christensen [121] were used for the radiolysis calculations on oxidative dissolution. The calculated and measured corrosion rates and gas-production rates are given in Table 7.

The calculated oxidative dissolution rates differ considerably, and the use of Ficks second law lowered the calculated rate nearly one order of magnitude. Assuming $A(\text{BET}) = 3 \times A(\text{geom.})$ and using the interfacial rate constants given in Table 5 we obtain a rate of 6.4 mg m^2 d^{-1}.

A similar combined transport and radiolysis model has recently been proposed by Poulesquen and Jegou [112]. The Chemsimul kinetic code is used for radiolytic calculations and the modelling of diffusive transport is based on Ficks second law. The α-dose rate profile is taken into account as input data. The reaction scheme used is the same as used by Christensen and Lundsröm [121,123].

Leaching experiments with high flux He^{2+} irradiation of a UO_2–water interface were simulated. The calculated uranium concentration was found to be three times lower and the H_2O_2 concentration ten times lower than the experimentally measured concentrations in aerated water. In deaerated water the calculated concentrations were two to three times lower than the experimental concentrations.

The calculations are very time consuming which reduces the usefulness of the code.

A compartment model to simulate H_2O_2 concentration profiles in water contacting spent fuel has been developed by Nielsen et al. [135]. The processes considered in the model are radiolytic H_2O_2 production by α- or a mixed α-/β-radiation field, H_2O_2 consumption in homogeneous and surface reactions, and diffusion. The simulations show that a steady state surface concentration is attained very quickly which simplifies the calculations of the

Table 6
Compartments and dose rates used in simulations.

Dist from fuel surface	Irradiated vol (cm^3)	α-doserate (Gy h^{-1})	β-doserate (Gy h^{-1})	γ-doserate (Gy h^{-1})
0–30 μm	0.013	1400	80,000	120
30 μm–3 mm	4.2	0	2200	120
3 mm–4.6 cm	200	0	0	80

Table 7
Calculated [121,123] and measured [137] dissolution rates.

Corrosion rate[a] (mg m^{-2} d^{-1})	H_2 (mol g^{-1} d^{-1})	O_2 (mol g^{-1} d^{-1})	Refs.
94	2×10^{-8}	1×10^{-8}	[121]
10			[123]
26	1.2×10^{-7}	9×10^{-8}	[137]

[a] 115 days.

maximum oxidative dissolution rate. In this context, it is important to note that the steady-state rate will be independent of the reaction mechanism employed for a pure and sealed system. If H_2O_2 is assumed to decompose to H_2O and O_2 to a large extent, then the O_2 concentration will increase until steady-state is reached. However, the steady-state level is still determined by the rate of H_2O_2 production. Consequently, identical steady-state dissolution rates will be attained regardless of the assumed relative rate constants for oxidation of UO_2. While this may not seem to be a problem in a pure and sealed system, the consequences in a more complex system where gases can escape and solutes reactive towards H_2O_2 and O_2 are present will be detrimental to the reliability of the calculation.

The radiolytic H_2O_2 production rate is given by:

$$r_{H_2O_2} = \int_{x=0}^{x_{max}} \dot{D}(x) \times \rho \times G(H_2O_2) dx \quad (37)$$

where $\dot{D}(x)$ is the dose rate at distance x from the fuel surface, ρ is the density of water and $G(H_2O_2)$ is the radiation chemical yield for H_2O_2. The maximum rate of the reaction between H_2O_2 and the UO_2 surface corresponds to the steady state where the rate of H_2O_2 consumption is identical to the rate of radiolytic H_2O_2 production. The steady-state surface concentration is calculated from Eq. (38)

$$[H_2O_2]_{s-s} = \frac{\overline{r_{H_2O_2}(\alpha)}\delta_{max}(\alpha) + \overline{r_{H_2O_2}(\beta)}\delta_{max}(\beta)}{k_{H_2O_2}} \quad (38)$$

where $\bar{r}$ is the average production rate in the irradiated volume (in mol dm^{-3} s^{-1}), δ is the maximum range of the radiation and $k_{H_2O_2}$ is the rate constant for the reaction between H_2O_2 and the fuel surface. The rate of spent nuclear fuel dissolution (taking the oxidation yield of 80% into account) is given by:

$$r_{diss} = r_{ox} = 0.8\left(\overline{r_{H_2O_2}(\alpha)}\delta_{max}(\alpha) + \overline{r_{H_2O_2}(\beta)}\delta_{max}(\beta)\right) \quad (39)$$

The combined effect of H_2 and ε-particles can also be accounted for using following equation:

$$r_{diss} = r_{ox} - k_{H_2}[H_2]\varepsilon_{rel} \quad (40)$$

The method has been extended to account for reactive solutes consuming H_2O_2 in solution [136].

The steady state model has been used to model spent fuel dissolution in 10 mM HCO_3^- solution [138]. In these experiments, oxidation rather than dissolution of the oxidized surface is expected to be rate determining. The calculated and experimental dissolution rates were found to agree within a factor of two.

Modelling of radiolysis effects on the oxidative dissolution of spent fuel has, as discussed above, been carried out using two different kinetic approaches. Christensen et al. [120] assumed a monolayer of U(IV) to be dissolved at the fuel/water interface and used homogenous rate constant for the reactions with radiolytically produced oxidants, while Jonsson et al. [139] based their reaction mechanism on experimentally determined interfacial rate constants and the fuel A/V ratio.

In the following we model, using both approaches and Maksima Chemist, some experimental results reported by Jegou et al. [76] and Stroes-Gascoyne et al. [64]. Jegou et al. [76] dissolved and leached polished discs of $^{(238/239)}$Pu doped UO_2 and spent fuel fragments in the absence and presence of an external gamma irradiation source. The radiation dose rates are given in Table 3. Oxidative dissolution was carried out in deionised water and U-concentrations determined after acidification. Here the dissolution of the α-doped UO_2 is modelled in the absence of γ-radiation, and in an air-saturated solution in a γ-radiation field. The modelling is based on the geometric surface areas and rate constants given in Table 5. The experimental and modelling data are given in Table 8.

Table 8
Experimental [76] and modelling data.

System	$[H_2O_2]$ (M)	U (mg m^{-2} d^{-1})		
		Experimental	Homogeneous	Interfacial
α-doped UO_2		0.2	0.49	0.15
γ-air sat.	1.2×10^{-4}	83	3.6	130

Oxidation in the γ-irradiated air-saturated system is determined by the steady state (1.2×10^{-4} mol dm^{-3}) H_2O_2 concentration. As can be seen, the rate of oxidative dissolution obtained by using homogenous rate constants and a dissolved monolayer is clearly an underestimation.

The steady state H_2O_2 concentration and the oxidative dissolution rate in the γ-irradiated air-saturated fuel fragment system were experimentally determined to be 1.2×10^{-4} mol dm^{-3} and 115 (mg m^{-2} d^{-1}), respectively, clearly showing that the steady state concentration for the γ-irradiation case is the determining factor.

Stroes-Gascoyne et al. [65] studied the oxidative dissolution of ^{238}Pu-doped UO_2-electrodes in 0.1 M carbonate solution. Very little U was found in the acid solutions used to strip U adsorbed on the reaction vessel walls, showing that the oxidized materials at the surfaces were effectively dissolved in the experiment. Since the roughness factor of the polished electrodes in these experiments was not known, the geometric surface area is used to model the experiments. The experimental and modelling data are given in Table 9.

In this case, both approaches yield reasonable U concentrations at the higher dose rate, while the approach based on interfacial rate constants more clearly predicts this concentration at the lower dose rate.

Suzuki et al. [75] studied the oxidative dissolution of colloidal UO_2(s) particles in aqueous solutions irradiated with α-particles from a cyclotron. The solutions were analysed for U and H_2O_2. The extent of surface oxidation of the UO_2(s) was calculated from the difference in H_2O_2 concentration measured in blank solutions and solutions containing the colloidal particles. The solutions contained 1 mol dm^{-3} NaCl and 4×10^{-2} mol dm^{-3} HCO_3^- in Ar-purged water at pH 8.5. The high concentration of Cl^- interferes with the spur radical recombination reactions, reducing $G(H_2O_2)$ to approximately 4.6×10^{-8} mol J^{-1} [75]. Assuming the radical

Table 9
Experimental [64] and modelling data.

Mean dose rate in irradiated sol. (Gy s^{-1})	Time (h)	U in solution (μg)		
		Exp	Homogeneous	Interfacial
3.5	1152	420.7	221	675
0.35	881	19.75	45	15.6

Table 10
Dissolution and oxidation rates of colloidal UO_2(s) particles in cyclotron irradiated aqueous solutions containing 1 mol dm^{-3} NaCl and 4×10^{-2} mol dm^{-3} HCO_3^- [140]. Calculated rates of oxidation assuming H_2O_2 to be the main oxidant.

Dose rate (Gy min^{-1})	SA/V (m^{-1})	U-dissolution experimental (mg (U) m^{-2} d^{-1})	UO_2(s) oxidation experimental (mg (U) m^{-2} d^{-1})	UO_2(s) oxidation calculated (mg (U) m^{-2} d^{-1})
76	4350	122.7	445.8	102.7
153	8701	51.4	170.9	171
103	10,235	69.7	108.5	105.7
110	29,769	24.9	30	54.3
154	34,030	7.9	19.9	70
154	79,755	3.8	8.5	33
83	140,745	5	10.7	10.3

products formed in the Cl^- spur reactions do not react with the colloid surfaces, we calculated the rate of $UO_2(s)$ oxidation using the rate constant 7.3×10^{-8} m s^{-1} [9] for the reaction of H_2O_2 with $UO_2(s)$. The experimental data for rates of U-dissolution and $UO_2(s)$ surface oxidation [140] are given in Table 10 with the calculated rates of oxidation.

While some discrepancies exist, the agreement between the calculated and experimentally determined rates of oxidation is reasonable indicating that the reactants formed in the spur radical scavenging reactions with Cl^- are probably not oxidizing the $UO_2(s)$ surface. It should be noted that the rate of oxidation 445.7 mg (U) m^{-2} d^{-1} given in Table 10 is approximately 1.5 times higher than the rate of H_2O_2 formation expected for this experimental dose rate.

4. Concluding remarks

Based on the analysis above, as expected, the use of measured interfacial rate constants in simulations of radiation induced dissolution of spent nuclear fuel are more reliable and give results in generally good agreement with experimental results compared to simulations where homogeneous rate constants are used. The use of spatial dose rate distributions is particularly important when simulating behaviour over short time periods. For longer times, the use of spatial distributions is less important. Even though the use of spatial dose rate distributions gives the most accurate results, such simulations are time consuming and, to date, simulations over time periods of relevance in safety analyses have only been performed based on electrochemical models.

The steady-state approach provides a simple but fairly accurate alternative, but errors in the reaction mechanism and in the kinetic parameters used may not be revealed by simple benchmarking. As shown in this review, simulations based on assumed rate constants and unrealistic mechanisms can still give results in fairly good agreement with experimental data. This is partly due to data fitting and partly due to the fact that the system reaches steady-state. In order to develop more reliable models, it is essential to strictly use experimentally determined rate constants and verified reaction mechanisms, irrespective of whether the approach adopted is chemical or electrochemical.

Acknowledgements

The Swedish Nuclear Fuel and Waste Management Company (SKB) is gratefully acknowledged for financial support. DWS's contribution was funded under the Industrial Research Chair agreement between the Canadian Natural Sciences and Engineering Research Council (NSERC, Ottawa) and the Canadian Nuclear Waste Management Organization (NWMO, Toronto).

References

[1] R.L. Segall, R.S.C. Smart, Oxide surfaces in solution, in: J. Nowotny, L.-C. Dufour (Eds.), Surface and Near-Surface Chemistry of Oxide Materials, Elsevier, Amsterdam, 1988, pp. 527–576.
[2] J.W.T. Spinks, R.J. Woods, An Introduction to Radiation Chemistry, third ed., John Wiley and Sons Inc., New York, 1990.
[3] D.W. Shoesmith, J. Nucl. Mater. 282 (2000) 1–31.
[4] I. Grenthe, F. Diego, F. Salvatore, G. Riccio, J. Chem. Soc., Dalt. Trans. 11 (1984) 2439–2443.
[5] D.W. Shoesmith, F. King, A Mixed Potential Model for the Prediction of the Effects of Alpha Radiolysis, Precipitation and Redox Processes on the Dissolution of Used Nuclear Fuel, Ontario Power Generation Report No.: 06819-REP-01200-0038R00, 1998.
[6] J.S. Goldik, The Electrochemistry of SIMFUEL in Alkaline Hydrogen Peroxide, Ph.D. Thesis, The University of Western Ontario, 2006.
[7] J. de Pablo, I. Casas, J. Gimenez, V. Marti, M.E. Torrero, J. Nucl. Mater. 232 (1996) 138.
[8] J. de Pablo, I. Casas, J. Jiminez, M. Molera, M. Rovira, L. Duro, J. Bruno, Geochim. Cosmochim. Acta 63 (1999) 3097.
[9] M.M. Hossain, E. Ekeroth, M. Jonsson, J. Nucl. Mater. 358 (2006) 202.
[10] D.J. Wronkiewicz et al., Uranium: Mineralogy, Geochemistry and the Environment, Mineralogical Society of America, Washington, DC, 1999, p. 475.
[11] Office of Civilian Radioactive Waste Management, CSNF Waste Form Degradation, ANL-EBS-MD-000015-Rev.o2, 2004.
[12] M. Amme, T. Wiss, H. Thiele, P. Boulet, H. Lang, J. Nucl. Mater 341 (2005) 209.
[13] B.G. Santos, J.J. Noel, D.W. Shoesmith, J. Nucl. Mater. 350 (2006) 320.
[14] P.C. Burns, R.C. Ewing, M.L. Miller, J. Nucl. Mater. 245 (1997) 1.
[15] P.C. Burns, K.M. Deely, S. Skanthakumar, Radiochim. Acta 92 (2004) 151.
[16] G. Choppin, J.O. Liljenzin, J. Rydberg, Radiochemistry and Nuclear Chemistry, Reed Educational and Professional Publishing Ltd., Oxford, 1995.
[17] A. Mozunder, Fundamentals of Radiation Chemistry, Academic Press, 1999.
[18] J.A. LaVerne, L. Tandon, J. Phys. Chem. B 106 (2002) 380–386.
[19] J.A. LaVerne, S.E. Bonnies, J. Phys. Chem. B 107 (2003) 7277–7280.
[20] J.A. LaVerne, L. Tandon, J. Phys. Chem. B 107 (2003) 13623–13628.
[21] J.A. LaVerne, J. Phys. Chem. B 109 (2005) 5395–5397.
[22] M. Jonsson, Radiation induced processes at solid–liquid interfaces, in: J.F. Wishart, B.S.M. Rao (Eds.), Recent Trends in Radiation Chemistry, World Scientific, 2010, pp. 301–323.
[23] R.D. Astumian, Z.A. Schelly, J. Am. Chem. Soc. 106 (1984) 304–308.
[24] A.J. Bard, L.R. Faulkner, Electrochemical Methods: Fundamentals and Applications, second ed., John Wiley and Sons, New York, 2001, p. 98.
[25] E. Ekeroth, M. Jonsson, J. Nucl. Mater. 322 (2003) 242–248.
[26] B.G. Santos, H.W. Nesbitt, J.J. Noel, D.W. Shoesmith, Electrochim. Acta 49 (2004) 1863.
[27] D.W. Shoesmith, M. Kolar, F. King, Corrosion 59 (2003) 802.
[28] F. King, M. Kolar, Mathematical Implementation of the Mixed Potential Model for Fuel Dissolution, Ontario Power Generation Report No.: 06819-REP-01200-10005 R00, 1999.
[29] C.R.S. Needes, M.J. Nicol, A Study of Redox Reactions at a UO_2 Surface, National Institute for Metallurgy, Johannesburg, South Africa, NIM No.: 7073, 1973.
[30] J.S. Goldik, J.J. Noel, D.W. Shoesmith, J. Electroanal. Chem. 582 (2005) 241.
[31] J.B. Hickey, Trans. Inst. Min. Metall. 89 (1980) C145.
[32] W.H. Hocking, J.S. Betteridge, D.W. Shoesmith, J. Electroanal. Chem. 379 (1994) 339.
[33] M. Jonsson, E. Ekeroth, O. Roth, Mater. Res. Soc. Symp. Proc. 807 (2004) 77–82.
[34] S. Nilsson, M. Jonsson, J. Nucl. Mater. 410 (2011) 89–93.
[35] D.E. Richardson, H. Yao, K.M. Frank, D.A. Bennett, J. Am. Chem. Soc. 122 (2000) 1729.
[36] M.M. Hossain, M. Jonsson, J. Nucl. Mater. 373 (2008) 190–193.
[37] M.E. Torrero, E. Baraj, J. de Pablo, J. Giménez, I. Casas, Int. J. Chem. Kinet. 29 (1997) 261.
[38] I. Casas, J. Giménez, V. Martí, M.E. Torrero, J. de Pablo, Radiochim. Acta 66/67 (1994) 23.
[39] D.W. Shoesmith, S. Sunder, M.G. Bailey, G.J. Wallance, Corros. Sci. 29 (1989) 1115.
[40] J. de Pablo, I. Cassas, F. Clarens, F. el Aamrani, M. Rovira, Mater. Res. Soc. Symp. Proc. 663 (2001) 409.
[41] D.W. Shoesmith, S. Sunder, AECL-10488, Atomic Energy of Canada Limited, 1991.
[42] F. Clarens, J. de Pablo, I. Díez-Pérez, I. Casas, J. Giménez, M. Rovira, Environ. Sci. Technol. 38 (2004) 6656.
[43] F. Clarens, J. de Pablo, I. Casas, J. Giménez, M. Rovira, J. Merino, E. Cera, J. Bruno, J. Quiñones, A. Martínez-Esparza, J. Nucl. Mater. 345 (2005) 225.
[44] J. Bruno et al., Mater. Res. Soc. Symp. Proc. 353 (1995) 601.
[45] J. Giménez, F. Clarens, I. Casas, M. Rovira, J. de Pablo, J. Nucl. Mater. 345 (2005) 232.
[46] W.J. Gray, S.A. Steward, J.C. Tait, D.W. Shoesmith, Radioactive Waste Manage. 4 (1994) 2597.
[47] J. de Pablo, I. Cassas, J. Giménez, M. Molera, M.E. Torrero, Mater. Res. Soc. Symp. Proc. 465 (1997) 535.
[48] S.N. Nguyen, H.C. Weed, H.R. Leider, R.B. Stout, Mater. Res. Soc. Symp. Proc. 257 (1992) 339.
[49] G.I. Park, H.K. Lee, J. Korean Nucl. Soc. 28 (1996) 349.
[50] S. Sunder, D.W. Shoesmith, R.J. Lemire, M.G. Bailey, G.J. Wallace, Corr. Sci. 32 (1991) 373.
[51] I. Casas, J. Giménez, V. Marti, M.E. Torrero, J. de Pablo, Mat. Res. Soc. Symp. Proc. 294 (1993) 61.
[52] M.J. Nicol, C.R.S. Needs, N.P. Finkelstein, in: A.R. Burkin (Ed.), Leaching Reduct. Hydrometall., IMM, London, 1973, p. 12.
[53] D.E. Grandstaff, Econ. Geol. 71 (1976) 1493.
[54] S.M. Peper, L.F. Brodnax, S.E. Field, R.A. Zehnder, S.N. Valdez, W.H. Runde, Ind. Eng. Chem. Res. 43 (2004) 8188.
[55] J.B. Hiskey, T. I. Min. Metall. 88 (1979) C145.
[56] O. Roth, M. Jonsson, Cent. Eur. J. Chem. 6 (2008) 1–14.
[57] I. Casas, J. De Pablo, F. Clarens, et al., Radiochim. Acta 97 (2009) 485–490.
[58] J.S. Goldik, J.J. Noel, D.W. Shoesmith, Electrochim. Acta 51 (2006) 3278.
[59] D.W. Shoesmith, Used Fuel and Uranium Dioxide Dissolution Studies – A Review, Nuclear Waste Management Organization Report, NWMO TR-2007-03, 2007.
[60] W.J. Gray, Mater. Res. Soc. Symp. Proc. 176 (1990) 141.
[61] V.V. Rondinella, Hj. Matzke, J. Cobos, T. Wiss, Mater. Res. Soc. Symp. Proc. 556 (1999) 447.

[62] V.V. Rondinella, Radiochim. Acta 88 (2000) 527–532.
[63] J. Cobos, L. Havela, V.V. Rondinella, J. de Pablo, T. Gouder, J.P. Glatz, P. Carbol, H. Matzke, Radiochim. Acta 90 (2002) 597–602.
[64] S. Stroes-Gascoyne, F. King, J.S. Betteridge, F. Garisto, Radiochim. Acta 90 (2002) 603–609.
[65] S. Stroes-Gascoyne, F. Garisto, J.S. Betteridge, J. Nucl. Mater. 346 (2005) 5–15.
[66] T. Mennecart, B. Grambow, M. Fattahi, Andriambololona, Radiochim. Acta 92 (2004) 611–615.
[67] D.W. Shoesmith, F. King, A Mixed Potential Model for the Prediction of the Effects of Alpha Radiolysis, Precipitation and Redox Processes on the Dissolution of Used Nuclear Fuel, Ontario Power Generation Report No.: 06819-REP-01200-0038 R00, 1998.
[68] C. Jegou, V. Broudic, A. Poulesquen, J.M. Bart, Mater. Res. Soc. Symp. Proc. 807 (2004) 391–396.
[69] P. Carbol, J. Cobos-Sabate, J.-P. Glatz, C. Ronchi, V. Rondinella, D.H. Wegen, T. Wiss, A. Loida, V. Metz, B. Kenzler, K. Spahiu, B. Grambow, J. Quinones, A. Martinez-Esparza Valiente, Swedish Nuclear Fuel and Waste Management Company Technical Report TR-0509.
[70] B. Muzeau, C. Jegou, F. Delaunay, V. Broudic, A. Brevet, H. Catalette, E. Simoni, C. Corbel, J. Alloys Comp. 467 (2009) 578–589.
[71] S. Sunder, D.W. Shoesmith, N.H. Miller, J. Nucl. Mater. 250 (1997) 66.
[72] S. Sunder, D.W. Shoesmith, M. Kolar, D.M. LeNeveu, J. Nucl. Mater. 250 (1997) 118.
[73] J.C. Wren, D.W. Shoesmith, S. Sunder, J. Electrochem. Soc. 152 (2005) B470.
[74] G. Sattonnay, C. Ardois, C. Corbel, J.F. Lucchini, M.F. Barthe, F. Garrido, D. Gosset, J. Nucl. Mater. 288 (2001) 11–19.
[75] T. Suzuki, A. Abdelouas, B. Grambow, T. Mennecart, G. Blondiaux, Radiochim. Acta 94 (2006) 567–573.
[76] C. Jegou, B. Muzeau, V. Broudic, S. Peuget, A. Poulesquen, D. Roudil, C. Corbel, J. Nucl. Mater. 341 (2005) 62–82.
[77] H. Kleykamp, J. Nucl. Mater. 131 (1985) 221.
[78] H. Kleykamp, Nucl. Technol. 80 (1988) 412.
[79] H. Kleykamp, J. Nucl. Mater. 167 (1989) 49.
[80] P. Fors, The Effect of Dissolved Hydrogen on Spent Nuclear Fuel Corrosion, Ph.D. Thesis, Chalmers University of Technology, Gothenburg, 2009.
[81] H. He, P.G. Keech, M.E. Broczkowski, J.J. Noel, D.W. Shoesmith, Can. J. Chem. 85 (2007) 702.
[82] R. Manzel, C.T. Walker, J. Nucl. Mater. 301 (2002) 170.
[83] P.G. Lucuta, R.A. Verrall, Hj. Matzke, B.J. Palmer, J. Nucl. Mater. 178 (1991) 48.
[84] Hj. Matzke, P.G. Lucuta, R.A. Verrall, J. Nucl. Mater 185 (1991) 292.
[85] P.G. Lucuta, B.J.F. Palmer, Hj. Matzke, D.S. Hartwig, in: Proc. Sec Int. Conf. on CANDU Fuel, vol. 132, 1989.
[86] G.J. Hyland, J. Ralph, High Temp. High Press. 15 (1983) 179.
[87] N.J. Dudney, R.L. Coble, H.L. Tuller, J. Am. Ceram. Soc. 64 (1981) 627.
[88] P.W. Winter, J. Nucl. Mater. 161 (1989) 38.
[89] V.M. Oversby, Uranium Dioxide, SIMFUEL, and Spent Fuel Dissolution Rates – A Review of Published Data, SKB Report TR-99-22, 1999.
[90] C. Jegou, S. Peuget, V. Brondic, D. Roudil, X. Deschanels, J.M. Bart, J. Nucl. Mater. 326 (2004) 144.
[91] B. Hansson, in: Proc. IHLLW Conf., Las Vegas, 2004, p. 144.
[92] L.E. Thomas, R.E. Einziger, H.C. Buchanan, J. Nucl. Mater. 201 (1993) 310.
[93] J.W. Choi, R.J. McEachern, P. Taylor, D.D. Wood, J. Nucl. Mater. 230 (1996) 250.
[94] J. Cobos, D. Papaiannou, J. Spino, M. Coquerelle, J. Alloys Comps. 271–273 (1998) 610.
[95] C. Poinssot, C. Ferry, M. Kelm, B. Grambow, A. Martinez-Esparza Valente, L. Johnson, Z. Andriambololona, J. Bruno, C. Cachoir, J.-M. Cavendon, H. Christensen, C. Corbel, C. Jegou, K. Lemmens, A. Loida, P. Lovera, F. Miserque, J. de Pablo, A. Poulesquen, J. Quinones, V. Rondinella, K. Spahiu, D. Wegen, Final Report of the European Project Spent Fuel Stability under Repository Conditions, European Commission Report CEA-R-6093, 2005.
[96] B. Grambow, A. Loida, A. Martinez-Esparza Valiente, P. Diaz-Arocas, J. de Pablo, J.L. Paul, G. Marx, J.-P. Glatz, K. Lemmens, K. Ollila, H. Christensen, European Commission Report, Nuclear Science and Technology, EUR 19140 EN, 2000.
[97] K. Spahiu, U.-B. Eklund, D. Cui, M. Lidstrom, Mater. Res. Soc. Symp. Proc. 13 (2002) 633.
[98] K. Spahiu, J. Devoy, D. Cui, M. Lindstrom, Radiochim. Acta 92 (2004) 597.
[99] K. Ollila, Y. Albinsson, V. Oversby, M. Cowper, Swedish Nuclear Fuel and Waste Management Company Technical Report TR-03-13, 2003.
[100] E. Cera, J. Bruno, L. Duro, T. Eriksen, Swedish Nuclear Fuel and Waste Management Company Technical Report TR-06-07, 2007.
[101] F. King, M. J. Quinn, N.H. Miller, Swedish Nuclear Fuel and Waste Management Company Technical Report TR-99-27, 1999.
[102] F. King, D.W. Shoesmith, Swedish Nuclear Fuel and Waste Management Company Technical Report TR-04-20, 2004.
[103] J.K. Norskov, T. Bligaard, A. Lagodittir, J.R. Kitchin, J.G. Chen, S. Pandelov, U. Stimming, J. Electrochem. Soc. 152 (2005) J23.
[104] M.E. Broczkowski, J.J. Noel, D.W. Shoesmith, J. Nucl. Mater. 346 (2005) 16–23.
[105] S. Nilsson, M. Jonsson, J. Nucl. Mater. 374 (2008) 290–292.
[106] M. Trummer, S. Nilsson, M. Jonsson, J. Nucl. Mater. 378 (2008) 55–59.
[107] T.E. Eriksen, M. Jonsson, J. Merino, J. Nucl. Mater. 375 (2008) 331–339.
[108] B. Pastina, J.A. LaVerne, J. Phys. Chem. A 105 (2001) 9316–9322.
[109] M. Trummer, M. Jonsson, J. Nucl. Mater. 396 (2010) 163–169.
[110] F. Garisto, Ann. Nucl., Energy 16 (1989) 33–38.
[111] F. Nielsen, M. Jonsson, J. Nucl. Mater. 359 (2006) 1–7.
[112] A. Poulesquen, C. Jegou, Nucl. Technol. 160 (2007) 337–345.
[113] L. Liu, I. Neretnieks, Nucl. Technol. 135 (2001) 273–285.
[114] D.W. Shoesmith, M. Kolar, Corrosion 59 (9) (2003) 802–816.
[115] F. King, M. Kolar, Ontario Power Generation Nuclear Waste Management Report, 06819-REP-01300-10019, 2000.
[116] B. Pastina, J.A. LaVerne, J. Phys. Chem. A 103 (1999) 209–212.
[117] B. Pastina, J.A. LaVerne, S.M. Pimblott, J. Phys. Chem. A 103 (1999) 5841–5846.
[118] I. Štefanić, J.A. LaVerne, J. Phys. Chem. A 106 (2002) 447–452.
[119] M. Kolar, F. King, Ontario Power Generation Report No.: 06819-REP-01200-10104-R00, 2003.
[120] H. Christensen, S. Sunder, D.W. Shoesmith, J. Alloys Comps. 213/214 (1994) 93–99.
[121] H. Christensen, Nucl. Technol. 124 (1998) 165–174.
[122] M. Kelm, E. Bohnert, Forschungszentrum Karlsruhe, FZKA 6977 (2004).
[123] T. Lundström, PhD-thesis, Linköping University, Dissertation No. 840, 2003.
[124] H. Christensen, E. Bjergbakke, Mater. Res. Soc. Symp. Proc. 84 (1987) 115.
[125] M.B .Carver, D.V. Hanley, K.R. Chaplin, MAKSIMA-CHEMIST, A Program for Mass Action Kinetics Simulations by Automatic Chemical Equation Manipulation and Integration Using Stiff Techniques, AECL-6413, Atomic Energy of Canada Limited, 1979.
[126] L.E. Eary, L.M. Cathles, Metall. Trans. B 148 (1983) 325.
[127] J. Merino, E. Cera, J. Bruno, J. Quinones, I. Casas, F. Clarens, J. Gimenez, J. de Pablo, M. Rovira, A. Martinez-Esperanta, J. Nucl. Mater. 346 (2005) 40–47.
[128] E. Ekeroth, O. Roth, M. Jonsson, J. Nucl. Mater. 355 (2006) 38–46.
[129] H. Christensen, R. Lindquist, L.O. Werme, SKB Report NS-90/85, 1990.
[130] D.W. Shoesmith et al., Ontario Power Generation Report No.: 06819-REP-01200-10145-R00, 2005.
[131] O. Roth, T. Bönnemark, M. Jonsson, J. Nucl. Mater. 353 (2006) 75–79.
[132] O. Roth, H. Hasselberg, M. Jonsson, J. Nucl. Mater. 383 (2009) 231–236.
[133] M. Trummer, O. Roth, M. Jonsson, J. Nucl. Mater. 383 (2009) 226–230.
[134] S. Sunder, N.H. Miller, D.W. Shoesmith, Corros. Sci. 46 (2004) 1095.
[135] F. Nielsen, K. Lundahl, M. Jonsson, J. Nucl. Mater. 372 (2008) 32–35.
[136] F. Nielsen, M. Jonsson, J. Nucl. Mater. 374 (2008) 281–285.
[137] A. Loida, B. Grambow, H. Geckeis, P. Dressler, Mater. Res. Soc. Symp. Proc. 353 (1995) 577.
[138] F. Nielsen, E. Ekeroth, T.E. Eriksen, M. Jonsson, J. Nucl. Mater. 374 (2008) 286–289.
[139] M. Jonsson, F. Nielsen, O. Roth, E. Ekeroth, M.M. Hossain, Environ. Sci. Technol. 41 (2007) 7087–7093.
[140] T. Suzuki, personal communication, 2009.